Fast event-related mapping of fingertip population receptive fields in human somatosensory and motor cortex at 7T

Sarah Khalife, B.Sc (1st Author)

Address: Department of Psychology, American University of Beirut, Beirut, Lebanon

Email: skk14@mail.aub.edu

Susan T. Francis, PhD

Address: Sir Peter Mansfield Imaging Centre, School of Physics and Astronomy, University of Nottingham, Nottingham, United Kingdom

Email: susan.francis@nottingham.ac.uk

Denis Schluppeck, PhD

Address: Visual Neuroscience Group, School of Psychology, University of Nottingham, Nottingham, United Kingdom

Email: denis.schluppeck@nottingham.ac.uk

Rosa-Maria Sánchez-Panchuelo, PhD

Address: Sir Peter Mansfield Imaging Centre, School of Physics and Astronomy, University of Nottingham, Nottingham, United Kingdom

Email: rosa.panchuelo@nottingham.ac.uk

Julien Besle, PhD (Corresponding Author)

Address: Department of Psychology, American University of Beirut, Beirut, Lebanon

Email: jb66@aub.edu.lb

Data Availability Statement:

The data that support the findings of this study are openly available in OpenNeuro at https://doi.org/10.18112/openneuro.ds003990.v1.0.2, reference number ds003990.

Funding Statement:

This work was supported by a BBSRC grant (BB/G008906/1) and by the University Research Board of the American University of Beirut. The funding sources had no involvement in the study design, collection, analysis and interpretation of data, writing of the manuscript or decision to submit the article for publication.

Conflict of Interest Disclosure:

The authors declare that they have no conflicts of interest.

Ethics Approval Statement:

Approval for the study was obtained from the University of Nottingham Ethics Committee.

Patient Consent Statement:

Informed consent was obtained from all subjects involved in the study.

Abstract

The majority of fMRI studies investigating somatotopic body representations in the human cortex have used either block or phase-encoding stimulation designs. Event-related (ER) designs allow for more natural and flexible stimulation sequences, while enabling the independent estimation of responses to different body parts in the same cortical location. Here we compared an efficiency-optimized fast ER design (2s inter stimulus interval, ISI) to a slow ER design (8s ISI) for mapping fingertip voxelwise tuning properties in the sensorimotor cortex of 6 participants at 7 Tesla. The fast ER design resulted in similar, but more robust, estimates compared to the slow ER design. Concatenating the fast and slow ER data, we demonstrate in each individual brain the existence of two separate somatotopically-organized representations of the fingertips, one in S1 on the post-central gyrus and the other at the border of the motor and pre-motor cortices on the pre-central gyrus. In both post-central and pre-central representations, fingertip tuning width increases progressively, from narrowly-tuned Brodmann areas 3b and 4a respectively, towards parietal and frontal regions responding equally to all fingertips.

Key Words

Ultra-high field fMRI; Somatosensory cortex; Event-related; Tactile perception; Population receptive field; Motor cortex

Key Points

- Fingertip population receptive fields (pRFs) in sensorimotor cortex can be efficiently mapped using a fast event-related design (ISI = 2 s) at 7T.
- Somatotopically-organized tactile maps were found not only in primary somatosensory cortex but also at the border between motor and premotor cortex.
- pRF size, reflecting the degree of integration between fingertips, increases from primary Brodmann areas 3b and 4a towards higher-order parietal and frontal regions.

1. Introduction

Mapping the details of somatotopic maps in the sensorimotor cortex is important for understanding tactile and motor information processing, both in the normal and diseased brain. The majority of fMRI studies that have mapped somatotopically-organized cortical representations in the somatosensory cortex have employed a phase-encoding (e.g. Puckett et al., 2017, 2020; Saadon-Grosman et al., 2020; Willoughby et al., 2020) or a block design (e.g. Pfannmöller et al., 2016; Schweisfurth et al., 2018), while very few studies have used event-related (ER) designs (Besle et al., 2014; Da Rocha Amaral et al., 2020; Valente et al., 2019). While phase-encoding designs are very efficient at mapping the dominant body part in a given cortical location, block and ER designs allow for the independent estimation of BOLD responses to the stimulation of different body parts in the same cortical location (Besle et al., 2014). This makes it possible to study how the cortical representations of different body parts overlap (Besle et al., 2014; Kolasinski et al., 2016b; Liu et al., 2021) and to measure local selectivity to different body parts (Besle et al., 2014; Martuzzi et al., 2014; Stringer et al., 2014), including the estimation of Gaussian population receptive fields (pRF) at the voxel level (Liu et al., 2021; Puckett et al., 2020; Saadon-Grosman et al., 2020a; Schellekens et al., 2018, 2021). Compared with ER designs, block designs are statistically more powerful at detecting differences between experimental conditions (Birn et al., 2002; Friston et al., 1999) and are therefore better suited if scanning time is a limiting factor. Event-related designs however present many advantages over block designs. First, they allow for more natural and flexible stimulation sequences and are more appropriate when studying transient cognitive processes involved in memory, attention, and other top-down effects (Huettel, 2012). Second, they allow the estimation of the hemodynamic response function and its comparison between experimental conditions (Birn et al., 2002; Dale, 1999; Liu, 2012).

Previous ER somatotopic mapping studies have used fairly long (random) intertrial intervals (e.g. Besle et al., 2014; Valente et al., 2019), resulting in non-optimal experimental designs. Efficiency can be improved by reducing the interstimulus interval (ISI), thereby increasing the number of trials and statistical power (Burock et al., 1998), but this also increases the temporal overlap in response to different trial types, potentially compromising the assumption of linearity underlying the most common types of fMRI analysis (e.g. GLM analysis), and therefore the accuracy of the response estimates (Heckman et al., 2007). Early tests of the assumption of linearity in the visual cortex suggested that it approximately holds for stimuli presented in short succession (Boynton et al., 1996; Dale and Buckner, 1997), but several subsequent studies have shown that rapid presentation can significantly alter the shape of the BOLD response in visual and motor cortex (e.g. Heckman et al., 2007; Miezin et al., 2000). The extent of possible departures from linearity in the tactile modality and how it might influence BOLD response estimation is currently unknown.

In this study, we acquired BOLD fMRI at 7 T to map the responses to tactile stimulations of the five fingertips of the left hand in 6 participants using either an efficiency-optimized fast ER design (2s intertrial interval) or a slow ER design (random 8s average intertrial interval). We show that both designs yield comparable somatotopic maps, hemodynamic responses, and tuning property estimates, but that estimates from the fast ER designs are significantly more reliable. Aggregating data across both types of ER designs, we characterize somatotopic maps and population receptive fields in both somatosensory and motor cortical systems and we replicate and extend results obtained across multiple recent studies that have used block or phase-encoding designs, including the existence of a small somatotopic representation of fingertips across motor and pre-motor cortex and an increase in fingertip pRF size from more primary Brodmann areas (BA) 3b and 4a to high-order areas in both parietal and frontal cortex.

2. Materials and Methods

The data that support the findings of this study are openly available in OpenNeuro at http://doi.org/10.18112/openneuro.ds003990.v1.0.2, reference number ds003990.

2.1. Subjects

Six right-handed neurotypical subjects participated in this study (aged 24–36 years, two females). Approval for the study was obtained from the University of Nottingham Ethics Committee. All subjects gave full written consent. Each

subject participated in three scanning sessions: two functional sessions at 7 T and one structural session at 3T. The latter was used to obtain a whole-brain T1-weighted volume for segmentation and cortical unfolding.

2.2. Tactile Stimulation and Functional Paradigms

Vibrotactile somatosensory stimuli were delivered to the fingertips of each participant's left hand by five independently controlled piezo-electric devices (Dancer Design, St. Helens, United Kingdom; http://www.dancerdesign.co.uk). The suprathreshold vibrotactile stimuli were applied to an area of approximately 1 mm^2 on the surface of the distal phalanges, at a frequency of 50 Hz.

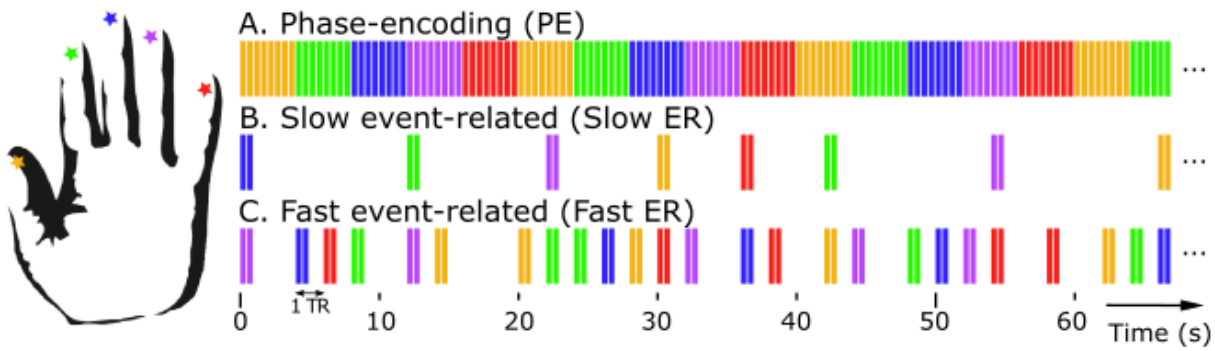

Figure 1: Fingertip stimulation sequence for the three experimental designs. In all three designs, stimulations were 400 ms, 50 Hz vibrotactile stimulation at the tip of the five fingers of the left hand (corresponding to the five colors in this figure). In the phase-encoding design (A), each fingertip was stimulated for 4 s (inter-stimulation interval = 100 ms) in clockwise (thumb to pinky, shown in this figure) or counter-clockwise order (not shown). In the slow and fast ER designs, each event consisted of two stimulations separated by 100 ms, but were presented in random order, with an inter-event interval of 4 to 12s in the slow ER design (B) or 2 s in the fast ER design (C). In addition, the fast ER sequence included 28% of null events.

Three different stimulation paradigms (Fig. 1) were used to assess the somatotopic representations in S1: (1) a phase-encoding localizer (Sanchez-Panchuelo et al., 2010), (2) a slow event-related (ER) design (Besle et al., 2014, 2013) and (3) a fast ER design, all acquired within the same scanning session. The phase-encoding localizer paradigm was used to estimate the location of each fingertip cortical representation in S1 for each subject. In this localizer, the five fingertips were stimulated for 4 s each in sequence (from thumb to pinky or pinky to thumb). Each 4 s stimulation period consisted in eight stimulations of 0.4 s separated by 0.1s gaps. The full stimulation cycle (4 s x 5 = 20 s) was repeated 9 times in two separate runs (one run from thumb to pinky and another in reverse order; see Besle et al., 2014 for details).

Following the phase-encoding localizer, four to six runs of each of the slow and fast ER designs were acquired in alternation (except for participant 5, for whom 10 fast and no slow ER runs were acquired). For both designs, each run consisted in a pseudo-random sequence of stimulations at the 5 fingertips. Each stimulation event consisted of two 0.4 s of 50 Hz stimulation to the same fingertip, separated by a 0.1 s gap. For each of the slow ER runs, six stimulation events were presented per fingertip, separated by a random onset-to-onset time interval of 2 to 6 TRs (4 to 12 s, in 2 s steps, total run duration around 230 s), with the constraint that the same fingertip could not be stimulated in consecutive events. For each of the fast ER runs, 18 stimulation events per fingertip and 36 null events were presented, separated from each other by one TR (2 s, total run duration = 242 s). Stimulation and null events were randomized by groups of 21 consecutive events (i.e. every 21 TR, there were exactly 6 null events and 3 stimulation events for each fingertip), as this was found to increase detection efficiency compared to fully randomized sequences (see below). In both slow and fast ER runs, the onset of a stimulation event always coincided with the start of an fMRI volume acquisition (TR) and the stimulation sequence ended before the end of the 252 s fMRI acquisition.

To maintain the participants' attention during ER sequences, subjects maintained fixation on a cross presented on a projection screen and performed a two-interval two-alternative forced-choice (2I-2AFC) tactile amplitude discrimination task on the fingertip stimulations. Participants were instructed to focus on stimulations at a single fingertip and ignore stimulations at all other fingertips. Their task was to report which of the two consecutive 0.4 s stimulation intervals at this fingertip had the highest amplitude by pressing one of two buttons with their non-stimulated, right hand. A visual verbal cue on a projection screen indicated to the participant what fingertip they should focus on. The indicated fingertip alternated every 40 s between the index and the ring finger, but events from each attentional focus condition will be averaged together in the present study and the corresponding attentional effect will be reported in a future study.

For fast ER runs, the random sequence of fingertip stimulation events was optimized to maximize detection efficiency. i.e. the efficiency of statistical contrasts testing for the response to each fingertip stimulation and baseline. Overall detection efficiency across fingertips was calculated as follows (Friston et al., 1999; Liu and Frank, 2004):

$$\text{efficiency} = \frac{1}{\frac{1}{5}\sum_{i=1}^{5} \; Tr\left(c_i \; \left(X^T X\right)^{-1} c_i \; \right)}$$

where $\boldsymbol{X}$ is the design matrix (the event matrix convolved with a canonical hemodynamic response function (HRF) modelled as a difference of Gamma functions) and $\boldsymbol{C}_i$ is the contrast matrix testing for a response to the stimulation of fingertip i compared to baseline. 50,000 sequences were drawn pseudo-randomly, and the 20 sequences with the highest overall detection efficiency were selected. Table 1 compares the detection efficiencies (first row) averaged across the 20 selected fast ER sequences to the average efficiency across 50,000 randomly drawn fast and slow ER sequences. While the randomly-drawn fast ER design sequences have detection efficiencies twice larger than the randomly-drawn slow ER design sequences, optimized fast ER sequences increased this advantage to a factor three. Table 1 also shows that randomizing the fast ER sequence over blocks of 21 events (instead of over the full run) and including null events, substantially increased detection efficiency.

In addition to detection efficiency, we also compared fast and slow ER runs in terms of their overall efficiency to estimate the HRF (Dale, 1999) and their overall efficiency to detect differences in activation between different fingertips. For the former, efficiency was computed by replacing the convolved design matrix with the stimulus convolution matrix (the Kronecker product of the event matrix with the identity matrix of size equal to the number of estimated HRF points (Dale et al., 1999; Liu and Frank, 2004)) and adjusting the contrast matrix accordingly. For the latter, efficiency was computed by keeping the convolved design matrix and averaging over the 10 contrasts corresponding to the 10 possible pairwise comparisons between fingertips. As can be seen in Table 1, the fast and slow ER design's HRF estimation and difference detection efficiencies differed by factors 2 and 3 respectively in favor of the fast ER design.

Contrast	**Fast ER (selected)**	**Fast ER (average)**	**Slow ER (average)**	**Fast ER (fully randomized)**	**fast ER (No null event)**
Detection (Fingertip vs baseline)	4.29 ± 0.49	2.95 ± 0.25	1.38 ± 0.09	2.41 ± 0.17	1.45 ± 0.03
HRF estimation	0.43 ± 0.02	0.43 ± 0.03	0.20 ± 0.02	0.38 ± 0.03	0.03 ± 0.00
Fingertip difference detection	2.77 ± 0.25	2.49 ± 0.22	0.97 ± 0.03	1.70 ± 0.10	1.82 ± 0.12

Table 1: Contrast efficiencies for different ER sequences of 5 fingertip stimulations. The leftmost column gives the average efficiencies for the fast ER sequences actually used in this study, selected amongst the 20 sequences with the largest detection efficiency (out of 50,000 randomly drawn sequences). The second and third columns give the average efficiency of randomly drawn sequences for the fast and slow ER designs. The fourth and fifth columns give the efficiencies of modified fast ER sequences, one in which events were randomized across the entire sequence instead of blocks of 21 events (4th column) and another that did not include null events (5th column). The three rows respectively correspond to overall efficiencies for detection contrasts (fingertip stimulation vs baseline, assuming a canonical HRF function), HRF estimation and difference detection contrasts (pairwise fingertip stimulation differences, also assuming a canonical HRF function). All e+nfficiencies are given with their respective standard deviation across 20 or 50,000 sequences.

This study also includes data collected in the same 6 subjects in a second functional session whose results have been published previously (Besle et al., 2014, 2013). This session (S2) was performed several weeks before the session described above (S1), and included only phase-encoding and slow ER runs (4 and 6 runs per participant respectively). In half of the slow ER runs, the participants' task was a 2I-2AFC tactile amplitude discrimination task similar to the one described above, except that participants had to respond irrespective of which fingertip was stimulated. In the other slow ER runs, participants performed a visual 2I-2AFC luminance discrimination task on the fixation cross (see Besle et al. 2013 for details). Again, data were averaged across attentional conditions for the present study.

2.3. Image Acquisition

Functional data were acquired on a 7 T scanner (Philips Achieva) with a volume-transmit coil and a 16-channel receiver coil (Nova Medical, Wilmington, MA). Foam padding and an MR-compatible vacuum pillow [B.u.W. Schmidt, Garbsen, Germany] were used to stabilize the participants' heads and minimize head motion artifacts. Functional data were acquired using T2*-weighted, multi-slice, single-shot gradient echo, 2D echo-planar imaging sequence (1.5 mm isotropic resolution, TR/TE = 2000/25 ms, FA = 75°, SENSE reduction factor 3 in the right-left (RL) direction), with a reduced FOV of 28 axial images covering the central part of the post-central and pre-central gyri (156 x 192 x 42/48 mm^3). Static B0 magnetic field inhomogeneity was minimized using an image-based shimming approach (Poole and Bowtell, 2008; Wilson et al., 2002) as described in Sanchez-Panchuelo et al. (2010). The functional runs were followed by the acquisition of high-resolution, T2*-weighted axial images (0.25 x 0.25 x 1.5 mm^3 resolution; TE/TR = 9.3/457 ms, FA = 32, SENSE factor = 2) with the same slice prescription and coverage as the functional data (in-plane).

For anatomical co-registration, subjects underwent high-resolution anatomical 3D MPRAGE imaging at 3 T (Philips Achieva, 1 mm isotropic resolution, linear phase encoding order, TE/TR= 3.7/8.13 ms, FA = 8°, TI = 960 ms). T1-weighted images were acquired on a 3 T as images display less B1-inhomogeneity-related intensity variation than 7 T data, thus improving tissue segmentation.

2.4. Preprocessing

Tissue segmentation and cortical reconstruction of the T1-weighted volumes were carried out using Freesurfer (http://surfer.nmr.mgh.harvard.edu/; (Dale et al., 1999)). Reconstructed cortical surfaces were flattened in a 60 mm radius patch around the expected location of the S1 hand representation on the post-central gyrus, using the mrFlatMesh algorithm (Vista software, http://white.stanford.edu/software/). Alignment of functional volumes to whole-head T1-weighted volumes was carried out using a combination of mrTools (Gardner et al., 2018) in MATLAB (The MathWorks, Natick, MA) and FSL (Smith et al., 2004). First, the high-resolution in-plane T2* volume was linearly aligned to the whole-head T1-weighted using mrTools' mrAlign (without resampling). Then, functional volumes were non-linearly registered and resampled to the high-resolution in-plane T2* volume using FSL fnirt (although at the original 1.5 mm^3 resolution of the functional volumes).

Alignment of the functional volumes (motion correction) was carried out using mrTools (mrAlign). Scanner drift and other low frequency signals were high-pass filtered (0.01 Hz cut-off) and data were converted to percent-signal change for subsequent statistical analysis. Analysis of functional data was performed using mrTools.

Freesurfer was used to estimate, for each participant, the location of primary and secondary sensorimotor Brodmann areas (BAs) 2, 1, 3b, 3a, 4a, 4p, and 6 from a probabilistic atlas based on the histological analysis of 10 post-mortem brains (Fischl et al., 2008). The maximum-probability map for these seven BAs was projected onto each participant's cortical surface using spherical normalization to a template surface. To define the BA borders that are not contiguous with any other BA in the atlas (e.g. the posterior border of BA 2 and the anterior border of BA 6), we thresholded the maximum probability map to a minimum of 50% probability.

2.5. Data analysis

All voxelwise analyses were conducted at the individual participant level in their respective native space (i.e. participant data were not spatially normalized and no voxel-wise group analyses were conducted). Group analyses were conducted after averaging voxel estimates across ROIs functionally defined on each participant's cortical surface.

2.5.1. Phase-encoding localizer

Phase-encoding localizer data were aggregated across the two functional sessions to maximise statistical power and were analyzed using conventional correlation analysis (Engel, 2012) to localize cortical regions responding preferentially to each fingertip stimulation (see details in Besle et al., 2013). Briefly, forward-order (thumb to pinky) phase-encoding time series were shifted backwards by k TRs to approximately compensate for hemodynamic delays, (with k chosen between 1 and 2 TRs depending on the participant). Reverse-order (pinky to thumb) phase-encoding time series were shifted by k+1 TRs and then time-reversed. Shifted forward-order time series and shifted, time-reversed, reverse-order time series were then separately concatenated across runs and the two concatenated time series were averaged samplewise. Finally, we computed, for each voxel, the sine phase of the 0.05Hz Fourier component (20 s period) of the averaged time series and its coherence (power at the 0.05 Hz frequency relative to all other frequency components). This procedure ensures that voxels preferring the thumb, index, middle, ring and pinky fingertips would have phases of exactly $\frac{\Pi}{5}$, $\frac{3\Pi}{5}$, Π, $\frac{7\Pi}{5}$ and $\frac{9\Pi}{5}$ respectively, irrespective of the hemodynamic delay (Besle et al., 2013). Coherence values were converted to p values under the assumption of independent Gaussian noise and p values were then corrected for multiple comparisons across voxels intersecting the 60 mm radius flattened cortical representation, using a stagewise Bonferroni method (Hommel, 1988).

After displaying the phase map on the flattened cortical patch and thresholding it at a corrected $p < 0.05$, we observed 2 somatotopically-organized regions in all participants, the largest extending from the post-central gyrus to the posterior bank of the central sulcus, corresponding to S1, and a smaller one on the pre-cental gyrus (see results section). We subdivided each of these two somatotopic regions into five fingertip-specific surface representations by selecting clusters of contiguous suprathreshold voxels in five contiguous $\frac{2\Pi}{5}$-wide phase bins between 0 and 2Π, i.e. contiguous regions responding preferentially to stimulation of each of the five fingertips. Fingertip-specific regions outside the two inferior-to-superior somatotopic representations (e.g. index representation located inferiorly to the thumb representation observed in a minority of participants) were not included. A third somatotopically-organized region was also observed in the fundus or the anterior bank of the central sulcus in some participants, but after checking on the volumetric data, we observed that each of its fingertip-specific regions is the continuation of a corresponding region in S1 through the central sulcus and therefore that this region may represent a spill-over from the posterior to the anterior bank of the central sulcus due either to extra-vascular BOLD responses or to co-registration error (see Supplementary Fig. 1).

2.5.2. Event Related design

2.5.2.1. Comparison of Slow and Fast ER design

To compare fingertip response estimates between the slow and fast ER designs, we first fitted separate GLM models to the data of each type of design. This analysis was done in only 5 participants since we acquired fast and slow ER runs in separate sessions for participant 5. All time series of a given design were concatenated and we fitted the GLM model to each concatenated dataset using a two-step approach that takes into account the shape and delay of each

participant's average hemodynamic response function (HRF) (Besle et al., 2013). In the first step, we estimated each participant's HRF by fitting a voxelwise deconvolution GLM, constructed by convolving the five sequences of fingertip stimulation events (one per fingertip) with 20 delta functions shifted by 1 TR (Gardner et al., 2005). The five obtained sets of 20 parameter estimates represent HRF estimates in response to each of the five fingertip stimulations over a duration of 40 s at each voxel. We then averaged these HRF estimates across all voxels of each S1 fingertip-specific representation, and finally averaged the HRF in response to the dominant fingertip of each representation across the five representations to obtain the participant's average HRF. In the second step, we fitted a voxelwise GLM model, constructed by convolving the five fingertip event sequences with the participant's average HRF estimated in the first step (normalized to unit integral), to obtain a single response estimate per fingertip stimulation (per voxel).

To compare the fingertip response estimates (both the HRF estimates from step 1 and the single response estimates from step 2) and their respective standard errors between the fast and slow ER designs at the group level, we averaged them across voxels of all five post-central fingertip-specific cortical representations for each participant. To avoid losing the finger specificity of these responses, averaging was done according to the fingertip preference of each cortical fingertip representation and finger adjacency: (1) average response to the preferred fingertip of each representation, (2) average response to fingertips directly adjacent to the preferred fingertip of each representation, (3) average responses to fingertips twice removed from the preferred fingertip of each representation, etc... For the single response estimates from step 2 of the GLM, this resulted in a tuning curve centred on the preferred fingertip. We estimated each participant's tuning curve's full width at half maximum (FWHM) by fitting a Gaussian centered on the preferred fingertip. To account for negative response estimates, the Gaussian was fitted with an offset parameter that could take only negative (or zero) values. The response estimate amplitudes and standard errors for the response to the preferred fingertip, as well as the fingertip tuning FWHM were compared between ER designs using paired t-tests.

To compare the hemodynamic delays between fast and slow ER designs, we also fitted the data with a GLM constructed by convolving the event sequences with a canonical double gamma HRF model (delay of first positive peak = 6 s, delay of second negative peak = 16 s, ratio of positive to negative peak = 6) and its time derivative. The ratio between the parameter estimate for the derivative and that of the double-gamma was used as a proxy for the HRF delay (larger values of the ratio correspond to a shorter delay) and compared between ER designs using t-tests.

Fingertip-specific response maps for each ER design were estimated by selecting voxels responding significantly more to a given fingertip stimulation than to the average of the other four fingertip stimulations. Statistical contrast maps were projected to the flattened cortical patch surrounding the central sulcus and we then created composite "preference" maps by overlaying the fingertip-specific maps for the five fingertips. Each fingertip-specific contrast map was thresholded at $p < 0.05$ using its corresponding p value map, corrected for multiple tests across voxels intersecting the flat cortical patch, using a step-up procedure controlling the false discovery rate (FDR) (Benjamini et al., 2006). In addition, the transparency of significant voxels in each map was set to be inversely proportional to the square-root of the negative logarithm of the corresponding FDR-adjusted p-values. All maps in this article are displayed averaged over the data intersecting the central 60% of the cortical sheet.

2.5.2.2. Characterization of Fingertip pRFs

To characterize pRFs in the somatosensory and motor cortex of each participant, we concatenated the data from both fast and slow ER designs, as well as with slow ER data from an additional session (see Tactile stimulation section). To estimate voxelwise pRF parameters, we first fitted the concatenated timeseries using the two-step GLM approach described previously which resulted in five fingertip response estimates per voxel (voxelwise tuning curves; Besle et al., 2019), and then fitted each voxel's tuning curve with a Gaussian function with two free parameters: the Gaussian mode/center (corresponding to the preferred fingertip) and the Gaussian spread (corresponding to fingertip tuning width), which we report as full width at half-maximum (FWHM) throughout this article. When fitting the Gaussian curve, the mode parameter was restricted to the [0.5 5.5] range in fingertip units (1=thumb; 5=little finger). The Gaussian spread parameter had a maximum permissible value of 30 fingertip units (maximum FWHM of $30 \times 2\sqrt{2ln2}$). Note that our method for estimating pRF parameters differs from other previously proposed estimation methods (e.g. Dumoulin and Wandell, 2008; Puckett et al., 2020) in that, instead of fitting a generative pRF model directly to the voxel timeseries, we first obtain the voxel's actual tuning curve using ordinary least-squares GLM and

then obtain the pRF parameters from the tuning curve. The pRF parameters are conceptually equivalent in both methods.

When displayed on the flat cortical patch, pRF center (preferred fingertip) maps were masked with the FDR-corrected p-value of an F test testing for the main effect of fingertip (any voxel having significantly different responses to at least one pair or fingertip stimulations, $p<0.05$). pRF width (fingertip tuning width) maps were thresholded using the FDR corrected p-value for an F testing for a significant positive response to the stimulation of at least one fingertip. FDR correction was applied across all voxels in the functional volume.

In addition to pRF parameter maps, we derived composite preference maps (see previous section), as well as composite "activation" maps highlighting the overlap between the responses to different fingertips (Besle et al., 2013, 2014). Composite activation maps were constructed similarly to preference maps, except that each overlaid fingertip map displays voxels that respond significantly to the stimulation of a given fingertip, compared to baseline and irrespective of the response to other fingertips. For voxels showing significant activation for several fingertips, the color was computed by combining the color of the different fingertip responses additively, resulting in a whitish hue for voxels responding to more than two fingertips (Besle et al., 2013).

2.5.2.3. Region of interest analysis

For group comparisons of pRF widths between different fingertip-specific cortical representations and between different regions of sensorimotor cortex, we defined ROIs based on a combination of functional criteria (fingertip preference from the phase-encoding analysis and statistical significance of the response relative to baseline from the ER analysis) and the maximum probability map of BAs projected to each participant's cortical surface (see Pre-processing section).

We grouped the five somatotopically-ordered post-central fingertip cortical representations into a single cortical region and then divided it according to cytoarchitectonic borders, obtaining three somatotopically-ordered post-central BA ROIs (3b, 1 and 2). We did the same for the pre-central fingertip cortical representation, obtaining two somatotopically-ordered pre-central BA ROIs (4a and 6). For regions responsive to tactile stimulation, but not somatotopically-organized, BA ROIs were defined by selecting clusters of significantly activated voxels responding significantly to the stimulation of at least one fingertip in the ER data ($p < 0.05$ FDR-corrected) within a given BA. For BA 3b, 1 and 4p, most responsive voxels were part of the region's somatotopic representation and so we did not define non-somatotopically-organized ROIs from these BAs. For BA2 and BA6, 80±6% and 10±3% of voxels were part of the post-central or pre-central somatotopic representation respectively, and we therefore defined two ROIs for each BA: one somatotopically-organized (described above and henceforth referred to as "ordered") and the other, not somatotopically-organized ("non-ordered"). All participants also showed a cluster of significantly activated voxels located posterior to BA2, which we named "Post-BA2" ROI. This ROI was spread across the post-central, intraparietal and parietal transverse sulci, as well as the parietal superior gyrus (in two participants, this ROI was composed of non-contiguous, but spatially close clusters, rather than a single contiguous cluster). We did not create ROIs for BA 3a or 4p (within the central sulcus) because fingertip-specific activity in these regions could generally be attributed to a "spill-over" of activation from BA 3b (see above and Supplementary Fig.1). Overall, we therefore defined five ordered BA ROIs (BA 3b, 1, 2, 4p and 6) and 3 non-ordered BA ROIs (post-BA2, BA2 and BA6) per participant.

In addition, for somatotopically-organized regions, we further divided each BA ROI into the five fingertip-specific ROIs. For the post-central ROIs, we only did this for BAs 3b and 1 because some participants did not show all five fingertip-specific representations in BA2. Similarly, for the pre-central ROIs, we grouped BA4a and BA6 ROIs together for each fingertip because not all fingertips were represented in both BA4a and BA6 in all participants. Overall, we therefore obtained 15 fingertip-specific ROIs, five in each of BA3b, BA1 and BA4a/6.

Fingertip tuning curves for the different ROIs were estimated by averaging all GLM-derived voxelwise tuning curves within a given ROI after recentering them on their respective pRF centers. Recentering the tuning curves was necessary to preserve the voxelwise tuning despite variation in fingertip preference across voxels in a given ROI (Besle et al., 2019). Without re-centering, the tuning of the average fingertip tuning curve within a somatotopically-

organized region such as ROI BA3b would be overestimated because this region contains voxels selective to each of the five fingertips. For recentering, voxelwise preferred fingertips were estimated from the phase encoding analysis, converting from the [0 2π] phase range to the [0.5 5.5] fingertip range and rounding to the nearest integer. It is important to use an independent dataset for the estimation of voxelwise fingertip preference for recentering (as opposed to using the pRF center estimated from the same ER-derived tuning curves) because this avoids biases due to circularity (see Supplementary Fig.2 for a comparison of ROI tuning curves obtained by recentering on the phase-encoding-derived or the ER-derived preferred fingertip). The resulting recentered ROI tuning curves thus consisted of 9 points, and were fitted with a Gaussian to obtain the ROI-averaged voxelwise tuning width (estimated as the FWHM of the best-fitting Gaussian). For this fit, the lower bound of the Gaussian spread parameter was set to 0.4 (minimum FWHM = $0.4 \times 2\sqrt{2ln2}$) to avoid unrealistically narrow tuning values. No upper bound was used.

To compare tuning widths between ROIs across participants, we used both the FWHM of Gaussian fitted to each participant's ROI tuning curves, and the ROI-averaged pRF width parameter. ROI tuning widths using either measure were compared across regions using one-way mixed-effect model ANOVAs. We conducted three separate analyses, one analysis including the 8 ordered and non-ordered BA ROIs, with ROI as a categorical variable (i.e. ignoring their anterior-posterior anatomical order), and two analyses with ROI as a continuous variable representing anterior-posterior location, including either only the post-central ROIs (1 = BA3b to 5 = post-BA2) or only BA3b and the pre-central BAs (1 = BA3b to 4 = non-ordered BA6). Post-hoc pairwise comparisons were corrected using Tukey's range test. As both measures of voxelwise tuning (FWHM of the ROI-average tuning curve or ROI-average pRF width) gave similar patterns of results, we only report results for the ROI-average pRF width. For fingertip-specific ROIs, ROI tuning widths were compared between BA ROIs (3a, 1 or 4a/6) and between the five fingertip stimulations using a two-way mixed-effect model ANOVA. Again, we conducted two separate analyses, one in which fingertip was considered a categorical variable and the other in which it was considered a numerical variable going from 1=thumb to 5=pinky.

2.5.2.4. Cortical magnification in fingertip-specific ROIs

We estimated magnification in a given somatotopically-organized BA ROI (3b, 1 and 4a/6) by measuring the geodesic cortical distance between the different fingertip-specific ROIs. To do this, we manually drew a line passing through the center of each fingertip-specific surface ROI in regions BA 3b, 1 and BA4a/6 and computed the average geodesic distance between all line vertices of each pair of consecutive fingertip ROIs.

3. Results

3.1. Comparison of Fast and Slow ER designs

To compare GLM-derived response estimates from the fast and slow event related (ER) designs (illustrated in Fig. 1B and C) we first delineated, in each participant, cortical regions responding preferentially to a single fingertip and located in the somatotopically-organized hand area of S1 on the post-central gyrus. These finger-specific cortical representations were delineated using a phase-encoding localizer (Fig. 1A). Based on the phase maps from this localizer (see Fig. 2 for participants 1-3 and Supplementary Fig. 3A for all participants), we identified two somatotopically-organized regions in all participants, one located on the contralateral (right) post-central gyrus, corresponding to S1, and a smaller one located on the contralateral pre-central gyrus. We estimated the location of cytoarchitectonic borders from a probabilistic atlas for each participant (dotted black lines in Fig. 2) and found that the S1 somatotopic representation spanned BA3b, 1 and 2 (46 ± 4%, 33 ± 2% and 21 ± 3% of voxels respectively), while the pre-central representation straddled the border between BA4 and BA6 (42 ± 5%, 49 ± 6% of voxels respectively). Both somatotopic regions had the same inferior-to-superior organization, going from thumb to pinky fingertip preference. Fingertip-specific cortical representations were delineated by grouping contiguous voxels with phase values corresponding to each fingertip and located within a somatotopically-organized region (see Methods section for details). All comparisons between the fast and slow ER response estimates were done on data aggregated across the 5 fingertip-specific cortical representations of the post-central S1 representation.

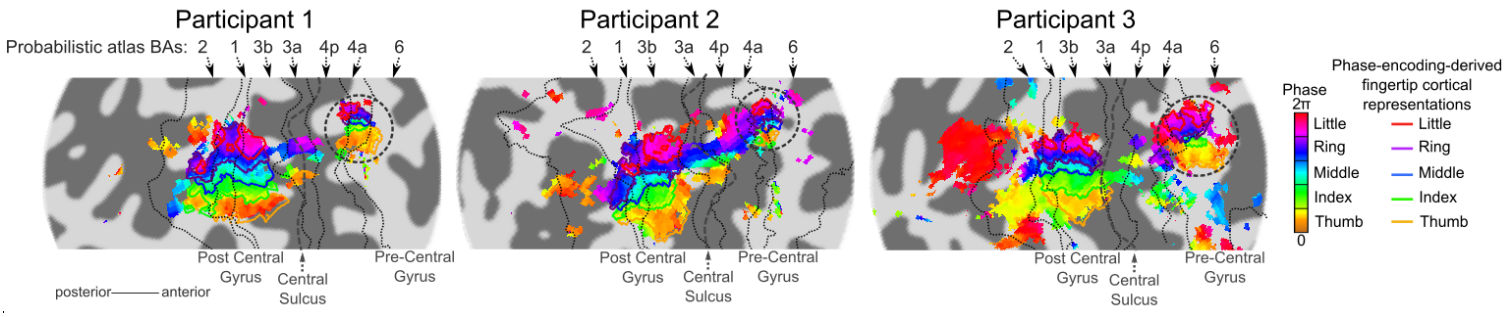

Figure 2: Fingertip-specific cortical representations in somatotopically-organized regions, as revealed by the phase-encoding design in participants 1-3 (see Supplementary Fig. 3A for all participants). Colored voxels show the phase of the sinewave best fitting the phase-encoding timeseries, with the correspondence between phase and fingertip preference shown in the color scale on the right. Phase maps were thresholded at a coherence value corresponding to $p < 0.05$, FDR-corrected. All participants showed two somatotopically-organized regions, one on the post-central gyrus and the other, smaller, on the pre-central gyrus (encircled with dotted outline). Some participants also showed hints of somatotopic responses in the central sulcus (BA 3a and 4p, but we cannot exclude that these were due to mis-registrations or extra-vascular BOLD response (See Supplementary Fig. 1). Fingertip-specific cortical representation on the post-central and pre-central gyri (colored outlines) were delineated by binning the phase values as indicated in the color scale and were used later on to define ROIs. Dotted black lines represent the likely location of borders between BAs, as derived from a probabilistic cytoarchitectonic atlas.

Figure 3A shows the group-average HRFs estimated in S1 from either the slow or the fast ER design, along with the corresponding voxelwise estimate standard errors. HRF estimates and standard errors were averaged across fingertip-specific S1 representations according to the fingertip preference of each cortical representation to preserve their fingertip tuning (see methods section for details). The estimated HRFs had broadly similar shapes and amplitudes between the two designs, with the HRF of the preferred fingertip about twice as large as that to fingertips directly adjacent to it, and responses to fingertips further away going slightly below baseline. However, the average voxelwise estimate standard errors were much smaller in the fast than in the slow ER designs, indicating more reliable estimates for the fast ER design. Despite broadly similar HRF shapes between the two designs, there were some minor differences: the HRFs from the fast ER design appear to have a slightly earlier peak with a less pronounced undershoot compared to those from the slow ER design. To statistically evaluate the difference in HRF peak, we fitted the data with a canonical double-gamma HRF model and its time derivative and compared the relative amplitude of the derivative HRF component between designs. While the relative amplitude of the time derivative was larger for the fast ER design, corresponding to an earlier HRF peak, this difference did not reach significance (Fast ER = 1.35 ± 0.38, Slow ER = 0.93 ± 0.21, $t(4) = 1.92$, $p = 0.127$, cohen's $d = 0.37$).

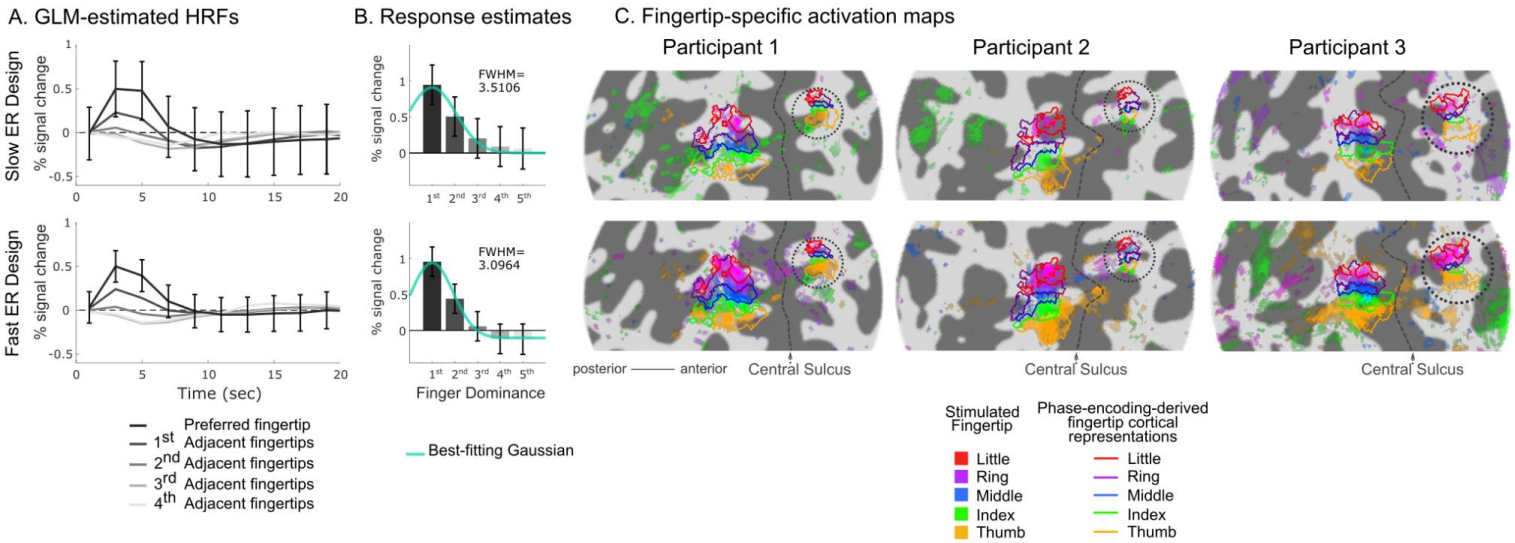

Figure 3: Comparison of response estimates and somatotopic maps between fast and slow ER designs. A: GLM-estimated HRF function averaged across the five fingertip-specific S1 cortical representations defined in Fig. 2, in response to the preferred and adjacent fingertips of each representation. Error bars represent the standard error of the voxelwise GLM estimates at each time point, averaged across voxels, cortical representations and participants. Estimate standard errors were smaller for the fast than the slow ER designs. B. Single-parameter response estimates for the preferred and adjacent fingertips, derived using a GLM analysis using the average participant-specific preferred-fingertip HRF as a canonical HRF. Again, parameter estimate standard errors were smaller in the fast than the slow ER design. C: Composite fingertip preference maps for each ER design in the first three participants. Each of the five colors represents voxels responding significantly more to a given fingertip than to the other four. Each fingertip map is thresholded at $p < 0.05$ FDR-corrected. Colored outlines represent the post-central and pre-central fingertip-specific cortical representations from the phase-encoding localizer. The number of significant voxels was much larger in the fast than the slow ER data.

To compare the selectivity (tuning width) of the fingertip response estimated from the two designs, we obtained single-value response estimates to each fingertip stimulation (preferred and different degrees of adjacency) by using the HRFs estimated for the preferred fingertip as canonical HRF models in the GLM fit (separately for each design). Figure 3B shows the obtained group-average fingertip tuning curves, averaged across fingertip-specific S1 cortical representations according to fingertip preference. Again, tuning curves obtained from the two different designs were broadly similar, but voxelwise estimate standard errors were significantly smaller for the fast than the slow ER design (tested only for the response to the preferred fingertip; Fast ER = 0.21 ± 0.04 % signal change, Slow ER = 0.3 ± 0.09, $t(4) = -2.8$, $p = 0.048$, $d = 1.26$). The two tuning curves had similar amplitudes at their maximum (i.e. in response to the stimulation of the preferred fingertip; Fast ER = 0.96 ± 0.0167 % signal change, Slow ER = 0.95 ± 0.136, $t(4) = 0.15$, $p = 0.88$, $d = 0.07$), but responses to fingertips away from the preferred fingertips were more negative (compared to baseline) for the fast than the slow ER design. As a consequence, the tuning curve was narrower for the fast than the slow ER design, as measured by the FWHM of best-fitting Gaussian, although this difference was not significant (Fast ER = 7.4 ± 0.7 fingertips, Slow ER = 9.4 ± 3.5, $t(4) = -1.13$, $p = 0.32$, $d = 0.5$). Overall, response estimates obtained using the fast and slow ER were therefore quite similar, despite small, non-significant, differences in HRF delay and tuning width, but fast ER estimates were more reliable (i.e. had significantly smaller voxelwise standard errors). This increased efficiency of the fast ER design can also be seen in the single-subject fingertip preference maps displayed in Figure 3C. These maps show voxels responding significantly more to the stimulation of a given fingertip than to the four others. While both designs yielded maps similar to the phase-encoding maps, preference maps obtained from the fast ER design showed many more significant voxels than those obtained from the slow ER design, both in S1 and in the smaller somatotopic representation on the pre-central gyrus.

3.2. Characterization of pRFs from ER data

Since response estimates were fairly similar when estimated from the fast and the slow ER design, we concatenated the two datasets together, as well as with data from an additional slow ER session with the same participants (Besle

et al. 2013, 2014). From this concatenated dataset, we characterized fingertip specificity in somatotopically-organized regions (S1 and pre-central region), as well as in other non-somatotopic, but responsive, regions.

Figure 4A shows composite maps of fingertip preference (showing voxels that respond significantly more to the stimulation of each fingertip compared to the four others) for three participants (see Supplementary Fig. 3B for all 6 participants). ER-derived preference maps showed the same pattern of ordered finger representations as the phase maps from the phase-encoding localizer (Fig. 2 and Supplementary Fig. 3A), both in S1 (BA 3b, 1 and 2) and on the pre-central gyrus (BA 4a and 6). One issue with preference maps (whether derived from phase-encoding or ER data) is that they only show voxels responding differentially to the stimulation of different fingertips, not voxels responding significantly but equally to all fingertips. Hence they underestimate the extent to which cortical fingertip representations overlap. Figure 4B shows composite maps of fingertip activation (showing voxels that respond significantly to the stimulation of each fingertip, compared to baseline). Composite activation maps reveal two features of the cortical representation that cannot be seen in the composite preference or phase-encoding maps. The first is that activation in response to fingertip stimulation extends much further than the somatotopically-organized regions seen on phase-encoding and composite preference maps. Many regions respond strongly to the stimulation of several fingertips (whitish regions in Fig. 4B), but do not show a strong preference for a particular fingertip and are not seen on maps that highlight fingertip preference. These regions are located posteriorly to the somatotopic S1 representation, either in BA2 or posterior to it, or anteriorly to the pre-central somatotopic representation, in BA6 or beyond. The second is that regions of strong fingertip specificity (corresponding mostly to the post-central and pre-central somatotopic representations) often in fact respond to two or more fingertips (seen in Fig. 4B as any voxel located within a fingertip-specific cortical representation, but not displaying a unique fingertip color). Different parts of the fingertip-specific cortical representations also seem to show different levels of overlap, with overlap more likely in the posterior part of the S1 somatotopic representation, mostly in BA2 and sometimes BA1, and in the pre-central fingertip-specific cortical representations (at least in some participants).

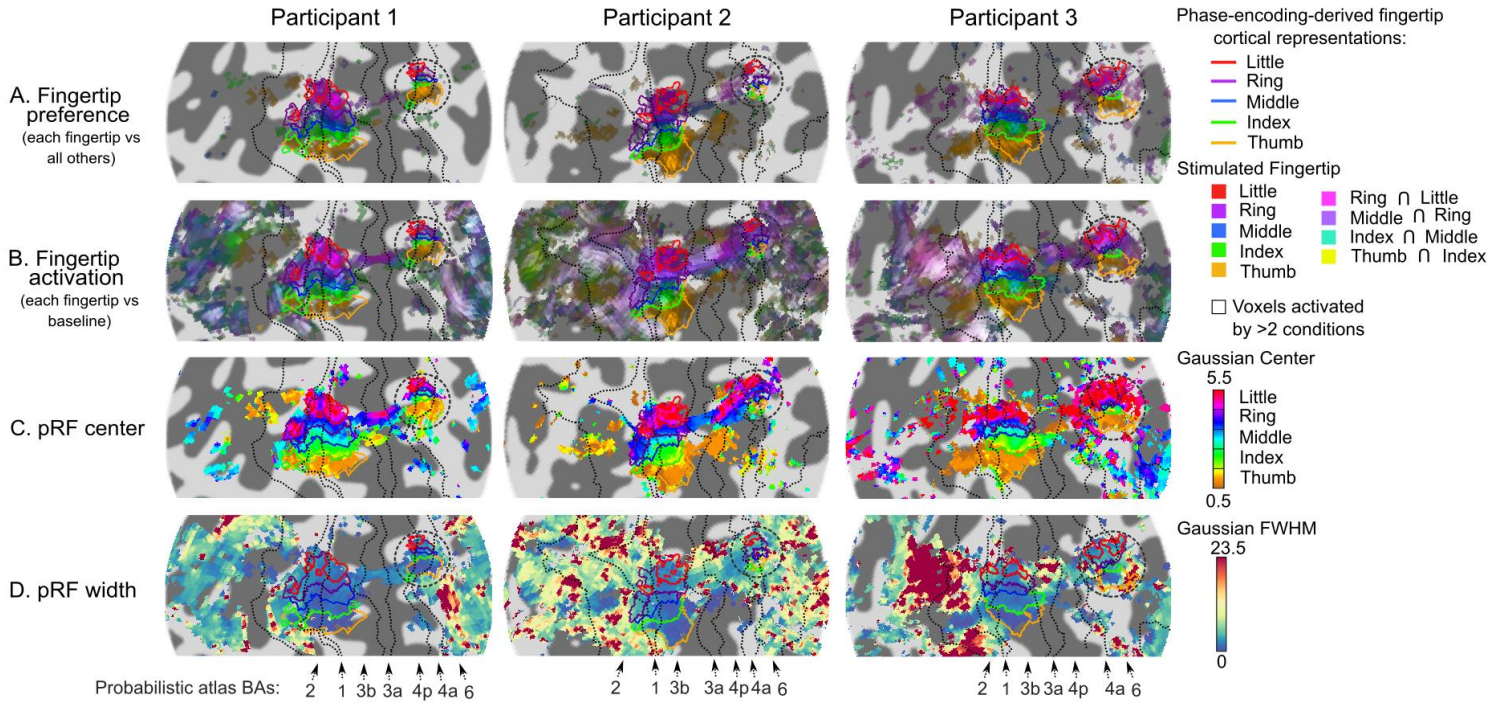

Figure 4: ER-derived single-subject maps of fingertip preference and selectivity in participants 1-3 (see Supplementary Fig. 3 for all participants). A. Composite fingertip preference maps showing which voxels respond more to a given fingertip stimulation than to the other fingertips on average, thresholded at $p < 0.05$ FDR-corrected for each fingertip contrast. This map highlights the same somatotopically-organized regions as the phase-encoding maps in Fig. 2. B. Composite activation maps showing which voxels respond significantly to the stimulation of each fingertip compared to baseline, thresholded at $p < 0.05$ FDR-corrected for each fingertip contrast. This map highlights voxels that responded significantly either mostly to one fingertip (same fingertip colors as

panel A), to two (usually adjacent) fingertips (blend of two fingertip colors) or more than two fingertips (white and off-white hues). C. Fingertip pRF center parameter maps computed by fitting voxelwise tuning curves with Gaussian, thresholded at $p < 0.05$ FDR-corrected according to the main effect of fingertip in the GLM analysis. This map highlights the same voxels as the phase-encoding (Fig. 2) and ER-derived composite preference maps (panel A). D. pRF width parameter maps (from the same fit as C), thresholded at $p < 0.05$ FDR-corrected according to an F-test testing for significant activation across any the five fingertips in the GLM analysis.

While composite activation maps show that many regions significantly respond to the stimulation of several fingertips, the degree of overlap shown in these maps may strongly depend on the chosen statistical threshold, and therefore on statistical power. To quantify the range of fingertips each voxel responds to (i.e. its fingertip tuning width), independently of statistical power, we fitted Gaussian population receptive field (pRF) models to the voxelwise GLM response estimates, with the pRF center parameter representing the preferred fingertip and pRF width/size parameter representing the fingertip tuning width of each voxel. Figures 4C and 4D respectively show pRF center and pRF width maps. Fingertip pRF center maps were essentially identical to both phase-encoding phase maps and composite preference maps, as expected. Fingertip pRF tuning width maps (Fig. 4D) show, also unsurprisingly, that somatotopically-organized post-central and pre-central regions had the narrowest tuning width (blue regions in Fig. 4D), and correspondingly the least overlap (compare with Fig. 4B), while non-somatotopic, tactile-responsive regions had the widest tuning (green to red regions in Fig. 4D). The post-central somatotopic region had similarly narrow tuning in all participants, at around 2-3 fingertips FWHM. In contrast, the pre-central somatotopic region's tuning width seemed to vary between participants, being as narrow as the post-central region in some participants (e.g participant 1) but more widely tuned in others (e.g. participant 2). Tuning width in non-somatotopically-organized regions posterior to the post-central gyrus or anterior to the central gyrus was larger, but also very variable across participants and regions.

To compare fingertip tuning width between different regions, and in particular between different putative cyto-architectonic areas, we divided the post-central and pre-central somatotopic regions in different BA ROIs according to the probabilistic cytoarchitectonic borders described previously. We then computed average voxelwise tuning curves in each of these five ROIs (BA2, 1, 3b, 4a and 6), as well as in non-somatotopic, but tactile-responsive, ROIs in BA6, BA2 and posterior to BA2 (Fig. 5A). ROI-averaged voxelwise tuning curves were obtained by averaging all voxelwise tuning curves within a given ROI, after centering them on their preferred fingertip to preserve the average voxelwise tuning (see Methods section for details). Somatotopically-organized regions in BA3b, 1, 2, 4a and 6 showed clearly tuned tuning curves, tapering off to baseline (or below) for fingertips away from the preferred fingertip, whereas non-somatotopic ROIs in BA6 and posterior to BA2 showed almost perfectly flat tuning curves with non-zero responses to all fingertips. Somatotopic regions showed marked differences in tuning width between the different BAs, with BA3b having the narrowest tuning (2.6 fingertips FWHM), increasing posteriorly to 4.0 and 9.3 in BA 1 and 2 respectively. Tuning widths in pre-central somatotopic BA4a and BA6 were similar to that in post-central BA1. Interestingly, the non-somatotopically-organized BA2 ROI showed some amount of tuning (FWHM = 18.9), although less than the ordered part of the BA. The increase in tuning width from BA3b posteriorly to BA2 and from BA4a anteriorly to the non-somatotopically-organized BA6 (Fig. 5B) were both statistically significant when assumed to be linear [$F(1, 23) = 49.33$; $p < 10^{-6}$ and $F(1, 17) = 52.68$; $p < 10^{-5}$ respectively]. There was also a significant main effect of ROI on tuning width [$F(7, 35) = 14.01$; $p < 10^{-7}$], but post-hoc pairwise comparisons were not significant between all pairs of ROIs (significant pairwise comparisons are reported in Fig. 5B).

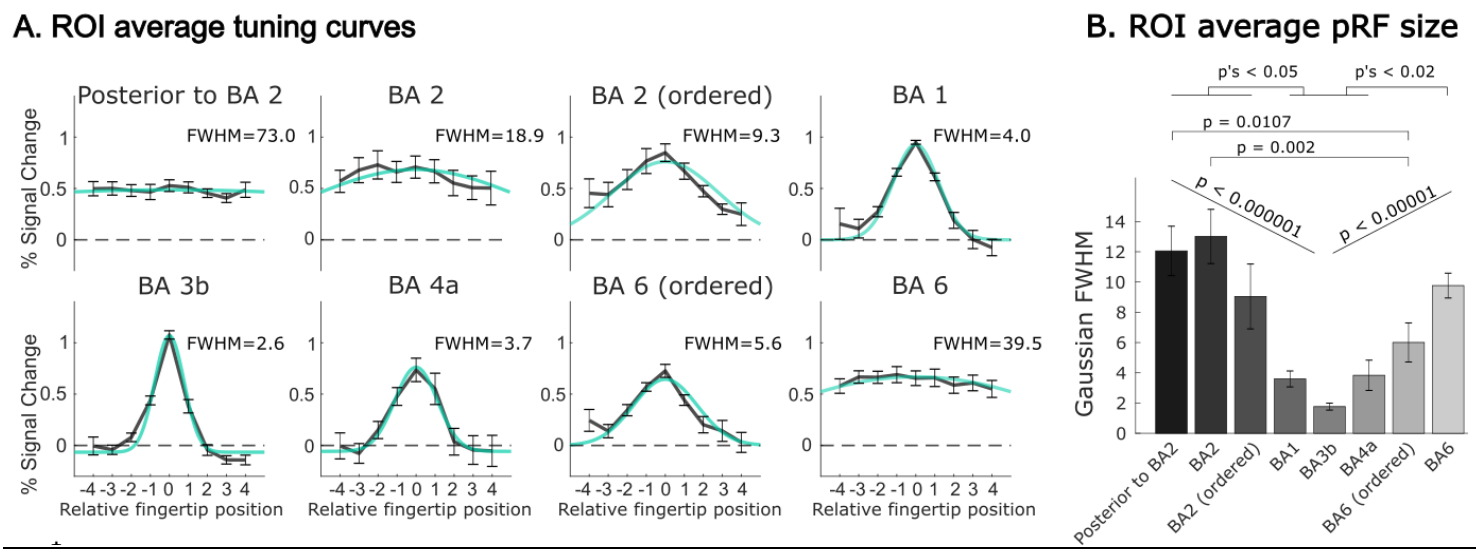

Figure 5: Voxelwise tuning curves and tuning widths in all somatotopically ordered and non-ordered ROIs, averaged across voxels in each ROI and across all participants. A. ROI-average voxelwise tuning curves with best-fitting Gaussian and associated Gaussian FWHM. Error bars represent the standard error of each ROI-average response estimate across participants. B. ROI-average pRF width parameter estimate, measuring fingertip tuning width. Error bars present the standard error of ROI-averaged pRF width estimates across participants. Horizontal bars indicate statistical significance for post-hoc pairwise comparisons, corrected for all possible pairwise comparisons. Both panels show that fingertip tuning width was smallest in BA3b and increased going posteriorly on the post-central gyrus and going anteriorly in the pre-central gyrus.

We also plotted ROI-average voxelwise tuning curves for each fingertip-specific representation in different somatotopic BAs (Fig. 6A) and compared tuning between these fingertip-specific ROIs (Fig. 6B). Figure 6A shows that responses were tuned in all fingertip-specific ROIs in BA3b, BA1 and BA4a/6, but that tuning width varied as a function of both fingertip and BA. The interaction between fingertip and BA was significant whether fingertip was considered a numerical variable (i.e. taking into account fingertip order and assuming a linear relationship between fingertip and tuning width; $F(2, 61.45) = 5.13$; $p = 0.008$) or a categorical variable (fingertip order was ignored; $F(1, 35) = 14.01$; $p = < 10^{-7}$). When fingertip was considered numerical, the interaction was due to tuning width significantly increasing from thumb to pinky in both BA3b and BA1, but not in ordered BA4a/6; however, when fingertip was considered categorical, not all pairwise comparisons between fingertips were significant in BA3b and BA1 (see detailed statistics in Fig. 6B). Despite the significant interaction between fingertip and BA, it was of interest to examine differences in tuning width between different BA ROIs irrespective of fingertip (main effect of BA). This analysis showed that fingertip tuning width was smaller in BA3b than in either BA1 ($p = 0.0570$) or BA4a/6 ($p = 0.0028$).

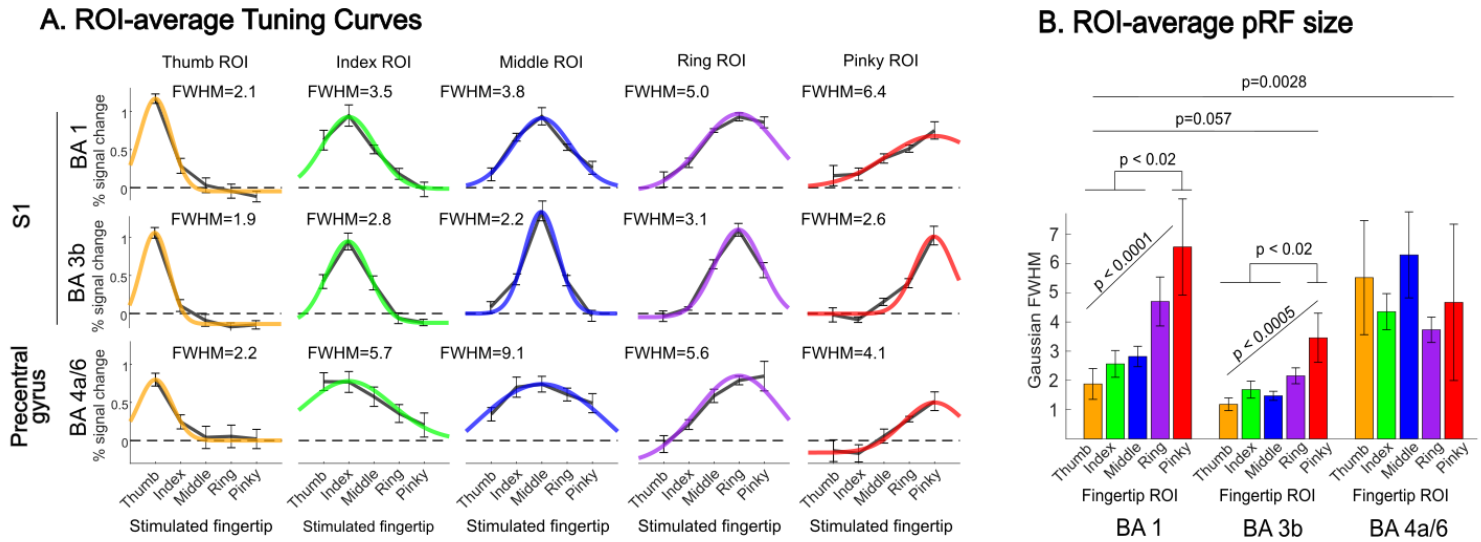

Figure 6: Voxelwise tuning curves and tuning widths in fingertip-specific ROIs in each somatotopically-organized BA. Panels A and B are as in Fig. 5, but for fingertip-specific regions divided by both fingertip stimulation preference and BA. Tuning width increased from the thumb to the pinky in BA3b and BA1, but not in BA 4a/6. BA3b was also more narrowly tuned than either BA1 or BA4a/6.

Finally, to verify whether tuning width across fingertips-specific representations and BAs are inversely related to cortical magnification, we estimated cortical magnification in somatotopically-organized BAs by calculating the geodesic distance between consecutive fingertip representations on the cortical surface (Fig. 7). The average cortical distance between the representations of adjacent fingertips was significantly larger in BA3b and BA1 than in BA4a/6 [Main effect of BA: $F(2,40) = 13.45$, $p < 10^{-4}$; BA3b = 4.7 ± 1.1 mm, BA1 = 4.8 ± 2.1 mm, BA4a/6 = 2.9 ± 1.1 mm; BA4a/6 vs BA3b: $t(10) = -4.414$, $p = 0.003$; BA4a/6 vs BA1: $t(10) = -4.33$, $p = 0.004$]. There was no main effect of fingertip pairs and no significant interaction between fingertip pairs and BA. Nevertheless, cortical distance between thumb and index representations seemed larger than between other consecutive pairs in BA3b and BA 4a/6 (but not in BA1).

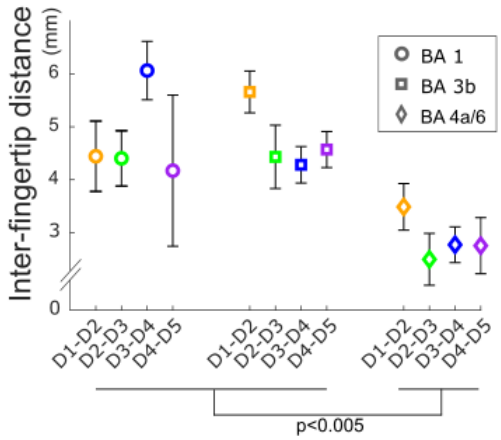

Figure 7: Cortical magnification functions in ordered BA ROIs. The cortical magnification functions were estimated by computing the geodesic cortical distances between consecutive pairs of adjacent fingertip ROIs in each BA. Error bars as in Fig. 5 and 6. There was no significant evidence for a cortical magnification in either of the three BAs (but the index-thumb distance was

larger than the other distances in BA3b and BA 4a/6). There was cortical magnification in post-central compared to pre-central ordered regions, in that distances were about twice as large in BA3b and BA1 than in the BA 4a/6.

---

4. Discussion

We have shown that at 7T responses to tactile stimulation of different fingertips can be mapped in detail in the sensorimotor cortex using a fast ER design. We demonstrate that an optimized fast (ISI=2 s) ER design is more efficient for characterizing response properties, such as the time-course of the HRF or fingertip specificity, than a slow (ISI=8 s) ER design, while differences in response property estimates are minimal between the two designs. Compared with phase-encoding designs, which emphasize regions that show a preference for specific body parts, ER designs allow for a more complete, yet flexible, mapping of response properties in cortex, including the evaluation of representational overlap and population receptive field parameters. This allows us to demonstrate the existence of a hierarchy of somatotopically-organized regions in both somatosensory and motor cortex presenting varying levels of representational integration: from somatotopically-organized regions responding specifically to a single or a few fingertips (including in motor cortex) to secondary regions responding equally to all fingertips.

4.1. Optimization of ER mapping sequences

Improving the efficiency of experimental designs for fMRI has been a long-standing endeavour and many different methods have been suggested to achieve efficient designs, including reducing the ISI or selecting the most efficient sequences from a large pool of randomly-drawn sequences, as we have done here (Burock et al., 1998; Dale, 1999; Friston et al., 1999). While optimized fast ER designs have been used in many domains of cognitive neuroscience, the actual efficiency gains have rarely been directly measured experimentally, in particular for designs with multiple trial types (five in our case). Since statistical efficiency calculations rely on assumptions (such as the linearity of the BOLD response) that might be incorrect in practice, it is not clear whether the actual gains will match those predicted. Here we empirically show that an efficiency-optimized fast ER sequence significantly reduces the uncertainty on fingertip stimulation response estimates compared to a random ER design with longer TRs (both when assuming a canonical HRF or when estimating the HRF). Actual efficiency gains afforded by the fast ER design (decrease in standard deviation by a factor 1.5) were lower than predicted by theoretical efficiency calculations (decrease by a factor 3), suggesting that some of the assumptions underpinning efficiency calculations might be violated for an ISI of 2 seconds.

GLM analyses of BOLD time series usually assume that the BOLD response is linear (Monti, 2011). Although this assumption is known to be violated for stimuli presented in quick succession (e.g. Wager et al., 2005), it has been claimed to be approximately correct for stimuli separated by several seconds in the visual cortex (Boynton et al., 1996). Our results suggest that BOLD responses to tactile stimulations presented 2 seconds apart add approximately linearly, since estimates were similar to those from a slower ER design, where the assumption is likely to hold. Nevertheless, slight differences in estimated HRF shape and fingertip tuning curve between the fast and slow designs indicates that reducing the ISI below 2 s to further increase statistical efficiency would probably introduce further biases. In the visual cortex, decreasing the ISI from 3 to 1 s has been shown to dramatically decrease the amplitude of the response, as well as the pattern of responses to different visual stimuli (Heckman et al., 2007). On balance therefore, an ISI of 2 s seems to provide a good trade-off between improved efficiency and estimation accuracy. A block design would be predicted to be even more efficient at detecting and differentiating responses to the stimulation of different fingertips, but at the cost of HRF estimation efficiency and experimental flexibility (see Introduction).

Our fast and slow ER sequences differed not only in their ISI value, but also in the fact that only the fast ER sequences were selected for efficiency out of a larger pool of random sequences. Therefore both factors (decreased ISI and selection out of a large pool) probably contributed to the observed improvement in efficiency. Our theoretical efficiency calculations suggest however that the decrease in ISI is a more important factor in improving efficiency (see Table 1). Further improvement in fast ER design efficiency could be obtained using alternative optimization strategies, such as m-sequences, whose efficiency exceeds that of the most efficient randomly-drawn sequence

(Buračas and Boynton, 2002), or the use of genetic algorithms (Wager and Nichols, 2003). Designs using overlapping stimulations of different fingers, such as multifocal mapping sequences (Vanni et al., 2005) could improve efficiency even further, but strongly rely on the assumption of additivity of responses to different fingertips. There is extensive evidence for non-linearities in the response to simultaneous stimulation of different fingertips in S1 (e.g. Arbuckle et al., 2021).

4.2. Fingertip pRF measurements in primary somatosensory cortex

We used a GLM analysis on the concatenated fast and slow ER data to derive voxelwise fingertip tuning curves (fingertip pRFs) (Besle et al., 2019), that we then fitted with Gaussian pRF models to derive preferred fingertip and tuning width maps. Fingertip pRF center maps agreed very well with phase-encoding-derived phase maps and demonstrated the existence of two somatotopically-organized regions: one at the probable location of S1, spanning BAs 3b, 1 and 2 on the posterior bank of the central sulcus and on the post-central gyrus, and a smaller region on the pre-central gyrus straddling BAs 4a and 6. The post-central representation is expected and has been mapped in many previous fMRI studies (e.g. Sanchez-Panchuelo et al., 2010). The smaller pre-central somatotopic representation will be discussed in more detail in section 4.2 of the discussion.

Fingertip tuning curves have previously been measured only in somatotopically-organized regions, either by averaging tuning curves across voxels in regions responding preferentially to the same fingertip (Besle et al., 2014, 2013; Martuzzi et al., 2014; Stringer et al., 2014; van der Zwaag et al., 2015), or by fitting Gaussian fingertip pRF models voxelwise (Liu et al., 2021; Puckett et al., 2020; Schellekens et al., 2018, 2021). Fitting pRF models voxelwise also allows the tuning width to be measured in regions that are not somatotopically-organized. Here we show that fingertip pRF width progressively increased from somatotopically-organized area BA3b, where tuning curves were the sharpest and voxels responded to a maximum of three adjacent fingertips, to non-somatotopic areas posterior to BA2, where tuning curves were flat and voxels responded equally to all fingertips. In addition, we find that tuning width in somatotopically-organized pre-central BA4a is similar to that in BA1, and increases anteriorly to a flat tuning curve in non-ordered parts of BA6. For the somatotopically-organized areas within S1, these results are consistent with fMRI studies that have shown both an increase in overlap between cortical representations of different fingertips going from anterior to posterior parts of S1 (Besle et al., 2014) and an increase in fingertip tuning width from BA3b to BA2 (Martuzzi et al., 2014; Puckett et al., 2020; Schellekens et al., 2021; Stringer et al., 2014). For pre-central areas, this is consistent with a recent fMRI study showing that the pRF width (at the coarser mapping scale of the entire body) increases not only posteriorly, but also anteriorly towards the pre-motor cortex, as we also observe here, as well as medially and laterally (Saadon-Grosman et al., 2020a). Flat tuning curves in areas posterior to S1 and in BA6 could reflect task-related processes that occur irrespective of the identity of the stimulated fingertip.

The increase in pRF width observed within S1 reflects a similar increase in neuronal fingertip receptive field width from BA3b to BA2 in non-human primates, probably reflecting integration of tactile information from increasingly larger skin surface area (review in Iwamura, 1998). However, the present BOLD-derived voxel pRFs most probably overestimate neuronal tuning width, since neuronal receptive fields in area 3b of non-human primates never encompass more than one fingertip (Nelson et al., 1980; Wang et al., 1995). This overestimation could be due either to variations in neurons' preferred stimulation location within a single voxel, or to the spatial spread of the BOLD response (Fracasso et al., 2021). Assuming that this spatial spread does not vary systematically across cortical areas, further increases in pRF width in other post-central or pre-central areas must be due either (or both) to an increase in the variability of neuronal fingertip preference within voxels, or to an increase in neuronal tuning width. The latter is consistent with neuronal receptive fields in the posterior part of S1 spreading across adjacent fingertips (Hyvärinen and Poranen, 1978; Iwamura, 1998).

Our quantitative estimates of BOLD-derived pRF width in S1 broadly agree with those previously reported by Schellekens et al. (2021) in BA3b and 1 (~2 fingertips FWHM in BA 3b and ~4 fingertips FWHM in BA1), but they were twice larger in BA2 in our study (~9 fingertips FWHM vs 4.5 fingertip FWHM in theirs). Wider pRFs in BA2 could be due to participants' performing an active discrimination task, compared to the passive tactile stimulation used by Schellekens et al. (2021). Performing a task might increase integration between information from different fingertips. However, pRF width estimates in these two studies are much lower than those from two previous studies

(Liu et al., 2021; Puckett et al., 2020) that reported fingertip pRF widths of ~9-10 fingertips FWHM on average across S1. Since one study used passive stimulation (Puckett et al., 2020) and the other used an active task (Liu et al., 2021), task differences cannot account for these larger pRF width estimates. Another possible explanation is that the two latter studies derived pRF parameters from phase-encoding stimulation sequences whereas both we and Schellekens et al. (2021) used pseudo-random stimulation sequences that included periods without stimulation (better suited to estimate pRF width in regions with large receptive fields because they allow the BOLD response to return to baseline; Dumoulin and Wandell, 2008). It is unclear however why deriving pRFs from phase-encoding stimulation sequences would result in larger (rather than smaller) pRF width estimates.

In addition to differences in average pRF width between cortical areas, we show that within somatotopically-organized BA3b and BA1, pRF width varies between the cortical representations of different fingertips, increasing overall from the thumb to the little finger. The pattern was compatible with a linear increase, as previously reported by Schellekens et al. (2021) (aggregated across BAs 3b, 1 and 2), but neither we nor they tested alternative models. When we tested for differences between pairwise cortical representations, the only significant differences were between the pinky and the thumb/index/middle fingertips in both BA3b and BA1. This is statistically similar to what was reported by Puckett et al. (2020), who reported similar pRF widths for the index/middle/ring representations (the thumb was not stimulated). While the increase in pRF width from thumb to little finger was monotonic in BA1, our data suggest a possible local pRF width maximum for the index fingertip representation in BA3b (not significant), similar to that reported in S1 by Liu et al. (2021) and found to be significant in their study. Therefore at this point, it is difficult to say whether pRF width increases monotonically from thumb to little finger representation or whether the pattern is more complex, at least in some BAs. Further studies measuring pRF width in more participants, providing more statistical power, are necessary to explore these questions. One important factor to control is handedness, as all other pRF studies stimulated the dominant (right) hand, but we stimulated the non-dominant (left) hand in this study.

Finally, in addition to the two somatotopic representations in S1 and the motor/premotor cortex, found in all participants, a subset of participants also showed partial or full somatotopic representations in BAs 3a and/or 4p, in the fundus or anterior bank of the central sulcus. When these existed however, we could not exclude that they corresponded to a spill-over from activation in BA3b through the sulcus, due either to extra-vascular BOLD contributions or to a slight misalignment of the functional and anatomical data (Supplementary Fig. 1). Somatotopic representation in the anterior bank or fundus of the central sulcus have been reported previously, in response to either passive tactile stimulation of different body parts (Saadon-Grosman et al., 2020b) or active movements of the limbs or fingers (Schellekens et al., 2018, 2020). None of these studies however examined the possibility that these pre-central somatotopic representations could be due to imperfect registration between functional and anatomical MRI data. Therefore it is premature to conclude that fingertip somatotopic maps exist in BA 3a or 4p.

4.3. Cortical magnification measurements in primary somatosensory cortex

If the cortical organization of somatosensory cortex follows the same principle as in the visual cortex, pRF width should be expected to be inversely related to the size of the cortical representation across fingertips (Harvey and Dumoulin, 2011), and therefore fingertips with smaller receptive fields would be expected to have larger cortical representations (i.e., be more magnified) than fingertips with larger receptive fields, perhaps reflecting a greater density of peripheral receptors on the skin surface of the thumb compared to the pinky. Our results are partially consistent with this expectation, since we found that the thumb-index cortical distance was greater than the cortical distances between other pairs of adjacent fingertips in BA3b. This difference however was not significant, possibly due to a lack of statistical power. In contrast, we found that the greatest cortical distance in BA1 was between the middle and ring fingertips (again, differences were not significant). The pattern of results in BA3b (but not in BA1) is compatible with those of previous studies that tested more participants. Liu et al. (2021) reported that the cortical geodesic distance between adjacent fingertip representations significantly decreases from thumb to pinky in S1 (but they did not test for differences between consecutive pairs). Similarly, Duncan and Boynton (2007) showed that the cortical distance between index, middle and ring fingers in S1 as a whole is greater than between ring and little fingers (the thumb was not stimulated). Other studies, measuring the Euclidean rather than the geodesic distance, reported a greater distance between thumb, index and middle finger than between ring and little finger, either in S1 overall

(Schweisfurth et al., 2018), or separately in BA3b and BA1 (Martuzzi et al., 2014). Euclidean distance measurements are not as accurate as geodesic distance measurements for measuring cortical distance however (Pfannmöller et al., 2016). Consistent with this, interdigit cortical distance shows a more regular increasing pattern from thumb to pinky when using geodesic rather than Euclidean distance (Liu et al., 2021). Therefore, although all results to date are compatible with more cortical magnification for the thumb, index (and maybe the middle finger) in at least BA 3b, the exact shape of the fingertip cortical magnification function is still unclear, as is the exact relationship between cortical magnification and pRF width. Cortical magnification in S1 as a whole has been found to be correlated tactile discrimination performance (Duncan and Boynton, 2007), although this correlation might be stronger in BA3b than in BA1 (Härtner et al., 2021).

4.4. Somatotopic representations in primary motor and premotor cortices

In addition to somatotopically-organized regions in BA3b and BA1, we demonstrate the existence of a small somatotopic representation of the fingertips at the border between the primary motor (BA4a) and pre-motor (BA6) areas. We have previously identified this region in three out of six participants in our previous publications using a subset of the present data (Besle et al., 2014, 2013), but the increased statistical power at the individual level allows us to confirm here that this map exists in all participants. The fact that the precentral region is somatotopically organized, shows fingertip tuning as narrow as in BA1, and is found in all six participants at approximately the same location suggests that it corresponds to a genuine somatotopic representation of fingertips in the motor cortex.

It has been debated whether there are fine somatotopic representations, e.g. at the level of fingertips, in motor cortex (Schieber, 2002; Schieber and Hibbard, 1993). Different regions of the hand representation in the motor or pre-motor cortex may instead represent typical hand movements involving multiple fingers (Ejaz et al., 2015; Graziano, 2016). Nevertheless, somatotopic ordering of fingers in motor cortex has been demonstrated by several fMRI studies using active motor tasks such as finger flexions/extensions, button press or finger tapping (Dechent and Frahm, 2003; Huber et al., 2020; Schellekens et al., 2018; Siero et al., 2014). While studies using active finger tasks have also often additionally reported somatotopically-organized responses in S1 (e.g. Huber et al., 2020; Kolasinski et al., 2016a; Sanders et al., 2019; Schellekens et al., 2018), studies using passive tactile stimulation of the fingertips like ours have only rarely reported somatotopic responses in the motor cortex. Aside from our previous reports (Besle et al., 2014, 2013), only one other study (to our knowledge) has reported somatotopically-organized tactile responses in the motor cortex (Saadon-Grosman et al., 2020b), although at the coarser scale of the entire body rather than fingertips. That somatotopic maps can be found in response to passive tactile stimulation is not necessarily surprising since many neurons in the motor system respond to tactile stimulation (e.g. Rizzolatti et al., 1988), although it has been unclear until now whether these sensory responses are somatotopically organized.

It is unclear at this point whether the present precentral somatotopic fingertip map corresponds to those previously reported in active motor task studies. The latter were usually attributed to locations in primary motor cortex (M1), but these studies did not in fact attempt to differentiate between primary motor cortex (BA4, located mostly in the anterior bank of the central sulcus) and pre-motor cortex (BA6, located mostly on the crown of the pre-central gyrus). In the few studies that displayed the somatotopic representation on the cortical surface (Dechent and Frahm, 2003; Sanders et al., 2019; Schellekens et al., 2018), the somatotopic map seems to span both the most superficial part of the anterior bank of the sulcus and the crown of the gyrus, which would be compatible with the location observed in our study (across BA4a and BA6). The inferior-superior location of the present fingertip map however does not seem to match that of previous active task studies. One study that mapped the somatotopic representation of fingertips in both M1 and S1 (Schellekens et al., 2018) found that they were directly facing each other across the central sulcus, forming quasi-continuous cortical bands spanning post-central, central and precentral regions. In contrast, we find that the pre-central representation is not only about twice smaller than the S1 representation but is also located more superiorly, with little suggestion of a continuity between the post-central S1 and the pre-central representations. The present somatotopic motor map also differs from some (but not all) previous active task studies in terms of size. The cortical distance between the centers of the thumb and pinky representations was about 10 mm in our study, similar to the size reported by (Dechent and Frahm, 2003; Siero et al., 2014), but smaller than the 15-20 mm reported by Schellekens et al. (2018) and larger than the 4-6 mm reported by Huber et al. (2020), who also reported two mirror reversed

somatotopic representations, in contrast with all previous studies reporting a single representation. Comparison of interfinger distances however is made difficult by important methodological differences across studies. Most previous studies measured euclidean distances along a single acquisition slice with arbitrary orientation relative to the cortical surface, rather than geodesic cortical distance as we did.

It is possible that there are multiple maps of fingertips in the motor system, since the primary motor and pre-motor cortical areas contain separate maps of hand movements (Graziano and Aflalo, 2007; Rizzolatti and Luppino, 2001). These different maps could be activated by different types of task (active movement vs passive tactile stimulation) or different types of executed movement (flexion vs extension vs tapping). Previous studies have suggested that activation in response to passive fingertip stimulation and active finger movements differ in both S1 and M1 (Berlot et al., 2019), and that different (mirror-reversed) somatotopic representations in M1 are co-located with responses to different types of movement (Huber et al., 2020).

4.5. Caveats

We showed that a fast ER design with an ISI of 2 s is more efficient than a slow (average ISI=8 s) ER design at mapping pRF properties in somatosensory cortex, but the pRF parameter maps and analyses we present in this article are based on data concatenated across two sessions that included one third of fast and two thirds of slow ER data, requiring a total acquisition time of ~60 minutes (excluding breaks, phase-encoding localizer and anatomical scans). Even with the increase in efficiency of the fast design, obtaining data of equivalent quality using only the fast ER design (and the same imaging parameters) would require 48 minutes of functional acquisition. This being said, the maps derived exclusively from fast ER data shown in Figure 3C took only 20 minutes to acquire and may be of sufficient quality for most uses.

The pRFs measured here were limited to the five fingertips that were stimulated in our experiment, but this doesn't mean that voxels in the hand regions of the sensorimotor cortex only respond to these five fingertips. To fully map pRFs in these regions would necessitate a much larger number of independently stimulated locations on other parts of the fingers and palm (see e.g. Wang et al., 2021), as well as the dorsum.

While we show both somatotopic and non-somatotopic fingertip responses in many regions of both the parietal and frontal lobe, our coverage was fairly limited in order to achieve a resolution of 1.5 mm with a reasonable TR (simultaneous multislice acquisition was not available at the time of acquisition). There may be other regions outside of the FOV used here that either contain somatotopic representations of the fingertips or the body as a whole, for instance S2 (Saadon-Grosman et al., 2020a; Sanchez Panchuelo et al., 2018), or respond equally to the stimulations of different body parts (have a flat tuning curve).

The locations of the cytoarchitectonic borders used to define ROIs in individual brains were derived from a probabilistic atlas, and so do not directly reflect the actual location of these borders in each participant. Their location accuracy on individual brains depends not only on the accuracy of the post-morterm cytoarchitectonic mapping used to derive this atlas (Fischl et al., 2008), but also on the assumption that this location can be predicted from gyral patterns, as this assumption underlies both the construction of the atlas and its projection to each individual brain. We cannot exclude that there may be systemic misolocalizations of some of these borders either because of inaccuracies in the original mapping, a violation of the above assumption, or sampling error either in the original post-morterm sample (N=10) or the present sample (N=6). For instance, it may seem surprising that the small pre-central somatotopic representation of fingertips was found at the border between BA4a and BA6, because somatotopic maps are usually understood to exist within a given area (although in S1, the same fingertip map is shared between BAs 3a, 3b, 1 and 2). A more accurate delineation of BAs could be obtained by mapping reversals in within-finger maps (Sanchez-Panchuelo et al., 2012), although it remains to be seen whether these reversals exist in the motor cortex, as they do in S1.

4.6. Conclusion

We have shown that a fast ER design (ISI = 2 s) can be used to map tactile fingertip pRF properties *in vivo* in the somatosensory, motor and premotor cortices of individual participants, with improved efficiency and minimal differences in estimates compared to a slower design (ISI = 8 s). Fingertip pRF properties in S1 were similar to those found previously using phase-encoding and block designs, but we also demonstrate the existence of a narrowly-tuned, somatotopically-organized tactile representation in motor/premotor cortex. Fast ER designs will likely play an important role in studying whether cognitive processes such as attention and memory can modulate tactile pRF properties in the sensorimotor cortex.

5. Author Contributions

Sarah Khalife: Formal analysis; Software; Visualization; Writing - original draft. **Susan Francis**: Conceptualization; Funding acquisition; Investigation; Methodology; Supervision; Writing - review & editing. **Denis Schluppeck**: Conceptualization; Funding acquisition; Investigation; Supervision; Writing - review & editing. **Rosa-María Sanchez Panchuelo**: Investigation; Methodology; Writing - review & editing. **Julien Besle**: Conceptualization; Formal analysis; Funding acquisition; Investigation; Software; Supervision; Writing - original draft; Writing - review & editing.

6. Funding

This work was supported by a BBSRC grant (BB/G008906/1) and by the University Research Board of the American University of Beirut. The funding sources had no involvement in the study design, collection, analysis and interpretation of data, writing of the manuscript or decision to submit the article for publication.

7. References

Arbuckle, S.A., Pruszynski, J.A., Diedrichsen, J., 2021. Mapping the integration of sensory information across fingers in human sensorimotor cortex. bioRxiv 2021.07.07.451552. https://doi.org/10.1101/2021.07.07.451552

Benjamini, Y., Krieger, A.M., Yekutieli, D., 2006. Adaptive linear step-up procedures that control the false discovery rate. Biometrika 93, 491–507. https://doi.org/10.1093/biomet/93.3.491

Berlot, E., Prichard, G., O'Reilly, J., Ejaz, N., Diedrichsen, J., 2019. Ipsilateral finger representations in the sensorimotor cortex are driven by active movement processes, not passive sensory input. J. Neurophysiol. 121, 418–426. https://doi.org/10.1152/jn.00439.2018

Besle, J., Mougin, O., Sánchez-Panchuelo, R.-M., Lanting, C., Gowland, P., Bowtell, R., Francis, S., Krumbholz, K., 2019. Is Human Auditory Cortex Organization Compatible With the Monkey Model? Contrary Evidence From Ultra-High-Field Functional and Structural MRI. Cereb. Cortex 29, 410–428. https://doi.org/10.1093/cercor/bhy267

Besle, J., Sánchez-Panchuelo, R.-M., Bowtell, R., Francis, S., Schluppeck, D., 2014. Event-related fMRI at 7T reveals overlapping cortical representations for adjacent fingertips in S1 of individual subjects. Hum. Brain Mapp. 35, 2027–2043. https://doi.org/10.1002/hbm.22310

Besle, J., Sánchez-Panchuelo, R.-M., Bowtell, R., Francis, S., Schluppeck, D., 2013. Single-subject fMRI mapping at 7 T of the representation of fingertips in S1: a comparison of event-related and phase-encoding designs. J. Neurophysiol. 109, 2293–2305. https://doi.org/10.1152/jn.00499.2012

Birn, R.M., Cox, R.W., Bandettini, P.A., 2002. Detection versus Estimation in Event-Related fMRI: Choosing the Optimal Stimulus Timing. NeuroImage 15, 252–264. https://doi.org/10.1006/nimg.2001.0964

Boynton, G.M., Engel, S.A., Glover, G.H., Heeger, D.J., 1996. Linear systems analysis of functional magnetic resonance imaging in human V1. J. Neurosci. Off. J. Soc. Neurosci. 16, 4207–4221.

Buračas, G.T., Boynton, G.M., 2002. Efficient Design of Event-Related fMRI Experiments Using M-Sequences. NeuroImage 16, 801–813. https://doi.org/10.1006/nimg.2002.1116

Burock, M.A., Buckner, R.L., Woldorff, M.G., Rosen, B.R., Dale, A.M., 1998. Randomized event-related experimental designs allow for extremely rapid presentation rates using functional MRI. Neuroreport 9, 3735–3739. https://doi.org/10.1097/00001756-199811160-00030

Da Rocha Amaral, S., Sanchez Panchuelo, R.M., Francis, S., 2020. A Data-Driven Multi-scale Technique for fMRI Mapping of the Human Somatosensory Cortex. Brain Topogr. 33, 22–36. https://doi.org/10.1007/s10548-019-00728-6

Dale, A., Buckner, R., 1997. Selective averaging of rapidly presented individual trials using fMRI. Hum Brain Mapp 5, 329–340. https://doi.org/10.1002/(sici)1097-0193(1997)5:5<329::aid-hbm1>3.0.co;2-5

Dale, A.M., 1999. Optimal experimental design for event-related fMRI. Hum. Brain Mapp. 8, 109–114. https://doi.org/10.1002/(SICI)1097-0193(1999)8:2/3<109::AID-HBM7>3.0.CO;2-W

Dale, A.M., Fischl, B., Sereno, M.I., 1999. Cortical Surface-Based Analysis: I. Segmentation and Surface Reconstruction. NeuroImage 9, 179–194. https://doi.org/10.1006/nimg.1998.0395

Dechent, P., Frahm, J., 2003. Functional somatotopy of finger representations in human primary motor cortex. Hum. Brain Mapp. 18, 272–283. https://doi.org/10.1002/hbm.10084

Dumoulin, S.O., Wandell, B.A., 2008. Population receptive field estimates in human visual cortex. NeuroImage 39, 647–660. https://doi.org/10.1016/j.neuroimage.2007.09.034

Duncan, R.O., Boynton, G.M., 2007. Tactile hyperacuity thresholds correlate with finger maps in primary somatosensory cortex (S1). Cereb. Cortex N. Y. N 1991 17, 2878–2891. https://doi.org/10.1093/cercor/bhm015

Ejaz, N., Hamada, M., Diedrichsen, J., 2015. Hand use predicts the structure of representations in sensorimotor cortex. Nat. Neurosci. 18, 1034–1040. https://doi.org/10.1038/nn.4038

Engel, S.A., 2012. The development and use of phase-encoded functional MRI designs. NeuroImage 62, 1195–1200. https://doi.org/10.1016/j.neuroimage.2011.09.059

Fischl, B., Rajendran, N., Busa, E., Augustinack, J., Hinds, O., Yeo, B.T.T., Mohlberg, H., Amunts, K., Zilles, K., 2008. Cortical Folding Patterns and Predicting Cytoarchitecture. Cereb. Cortex 18, 1973–1980. https://doi.org/10.1093/cercor/bhm225

Fracasso, A., Dumoulin, S.O., Petridou, N., 2021. Point-spread function of the BOLD response across columns and cortical depth in human extra-striate cortex. Prog. Neurobiol. 202, 102034. https://doi.org/10.1016/j.pneurobio.2021.102034

Friston, K.J., Zarahn, E., Josephs, O., Henson, R.N., Dale, A.M., 1999. Stochastic designs in event-related fMRI. NeuroImage 10, 607–619. https://doi.org/10.1006/nimg.1999.0498

Gardner, J.L., Merriam, E.P., Schluppeck, D., Besle, J., Heeger, D.J., 2018. mrTools: Analysis and visualization package for functional magnetic resonance imaging data. https://doi.org/10.5281/zenodo.1299483

Gardner, J.L., Sun, P., Waggoner, R.A., Ueno, K., Tanaka, K., Cheng, K., 2005. Contrast adaptation and representation in human early visual cortex. Neuron 47, 607–620. https://doi.org/10.1016/j.neuron.2005.07.016

Graziano, M.S.A., 2016. Ethological Action Maps: A Paradigm Shift for the Motor Cortex. Trends Cogn. Sci. 20, 121–132. https://doi.org/10.1016/j.tics.2015.10.008

Graziano, M.S.A., Aflalo, T.N., 2007. Mapping Behavioral Repertoire onto the Cortex. Neuron 56, 239–251. https://doi.org/10.1016/j.neuron.2007.09.013

Härtner, J., Strauss, S., Pfannmöller, J., Lotze, M., 2021. Tactile acuity of fingertips and hand representation size in human Area 3b and Area 1 of the primary somatosensory cortex. NeuroImage 232, 117912. https://doi.org/10.1016/j.neuroimage.2021.117912

Harvey, B.M., Dumoulin, S.O., 2011. The Relationship between Cortical Magnification Factor and Population Receptive Field Size in Human Visual Cortex: Constancies in Cortical Architecture. J. Neurosci. 31, 13604–13612. https://doi.org/10.1523/JNEUROSCI.2572-11.2011

Heckman, G.M., Bouvier, S.E., Carr, V.A., Harley, E.M., Cardinal, K.S., Engel, S.A., 2007. Nonlinearities in rapid event-related fMRI explained by stimulus scaling. NeuroImage 34, 651–660. https://doi.org/10.1016/j.neuroimage.2006.09.038

Hommel, G., 1988. A stagewise rejective multiple test procedure based on a modified Bonferroni test. Biometrika 75, 383–386. https://doi.org/10.1093/biomet/75.2.383

Huber, L., Finn, E.S., Handwerker, D.A., Bönstrup, M., Glen, D.R., Kashyap, S., Ivanov, D., Petridou, N., Marrett, S., Goense, J., Poser, B.A., Bandettini, P.A., 2020. Sub-millimeter fMRI reveals multiple topographical digit representations that form action maps in human motor cortex. NeuroImage 208, 116463. https://doi.org/10.1016/j.neuroimage.2019.116463

Huettel, S.A., 2012. Event-related fMRI in cognition. NeuroImage 62, 1152–1156.

https://doi.org/10.1016/j.neuroimage.2011.08.113
Hyvärinen, J., Poranen, A., 1978. Receptive field integration and submodality convergence in the hand area of the post-central gyrus of the alert monkey. J. Physiol. 283, 539–556.
Iwamura, Y., 1998. Hierarchical somatosensory processing. Curr. Opin. Neurobiol. 8, 522–528. https://doi.org/10.1016/S0959-4388(98)80041-X
Kolasinski, J., Makin, T.R., Jbabdi, S., Clare, S., Stagg, C.J., Johansen-Berg, H., 2016a. Investigating the Stability of Fine-Grain Digit Somatotopy in Individual Human Participants. J. Neurosci. 36, 1113–1127. https://doi.org/10.1523/JNEUROSCI.1742-15.2016
Kolasinski, J., Makin, T.R., Logan, J.P., Jbabdi, S., Clare, S., Stagg, C.J., Johansen-Berg, H., 2016b. Perceptually relevant remapping of human somatotopy in 24 hours. eLife 5, e17280. https://doi.org/10.7554/eLife.17280
Liu, P., Chrysidou, A., Doehler, J., Hebart, M.N., Wolbers, T., Kuehn, E., 2021. The organizational principles of de-differentiated topographic maps in somatosensory cortex. eLife 10. https://doi.org/10.7554/eLife.60090
Liu, T.T., 2012. The development of event-related fMRI designs. NeuroImage 62, 1157–1162. https://doi.org/10.1016/j.neuroimage.2011.10.008
Liu, T.T., Frank, L.R., 2004. Efficiency, power, and entropy in event-related FMRI with multiple trial types. Part I: theory. NeuroImage 21, 387–400. https://doi.org/10.1016/j.neuroimage.2003.09.030
Martuzzi, R., Zwaag, W. van der, Farthouat, J., Gruetter, R., Blanke, O., 2014. Human finger somatotopy in areas 3b, 1, and 2: A 7T fMRI study using a natural stimulus. Hum. Brain Mapp. 35, 213–226. https://doi.org/10.1002/hbm.22172
Miezin, F.M., Maccotta, L., Ollinger, J.M., Petersen, S., Buckner, R.L., 2000. Characterizing the Hemodynamic Response: Effects of Presentation Rate, Sampling Procedure, and the Possibility of Ordering Brain Activity Based on Relative Timing. NeuroImage 11, 735–759. https://doi.org/10.1006/nimg.2000.0568
Monti, M., 2011. Statistical Analysis of fMRI Time-Series: A Critical Review of the GLM Approach. Front. Hum. Neurosci. 5, 28. https://doi.org/10.3389/fnhum.2011.00028
Nelson, R.J., Sur, M., Felleman, D.J., Kaas, J.H., 1980. Representations of the body surface in postcentral parietal cortex of Macaca fascicularis. J. Comp. Neurol. 192, 611–643. https://doi.org/10.1002/cne.901920402
Pfannmöller, J.P., Greiner, M., Balasubramanian, M., Lotze, M., 2016. High-resolution fMRI investigations of the fingertip somatotopy and variability in BA3b and BA1 of the primary somatosensory cortex. Neuroscience 339, 667–677. https://doi.org/10.1016/j.neuroscience.2016.10.036
Poole, M., Bowtell, R., 2008. Volume parcellation for improved dynamic shimming. Magma N. Y. N 21, 31–40. https://doi.org/10.1007/s10334-007-0102-2
Puckett, A.M., Bollmann, S., Barth, M., Cunnington, R., 2017. Measuring the effects of attention to individual fingertips in somatosensory cortex using ultra-high field (7T) fMRI. NeuroImage 161, 179–187. https://doi.org/10.1016/j.neuroimage.2017.08.014
Puckett, A.M., Bollmann, S., Junday, K., Barth, M., Cunnington, R., 2020. Bayesian population receptive field modeling in human somatosensory cortex. NeuroImage 208, 116465. https://doi.org/10.1016/j.neuroimage.2019.116465
Rizzolatti, G., Camarda, R., Fogassi, L., Gentilucci, M., Luppino, G., Matelli, M., 1988. Functional organization of inferior area 6 in the macaque monkey. II. Area F5 and the control of distal movements. Exp. Brain Res. 71, 491–507. https://doi.org/10.1007/BF00248742
Rizzolatti, G., Luppino, G., 2001. The Cortical Motor System. Neuron 31, 889–901. https://doi.org/10.1016/S0896-6273(01)00423-8
Saadon-Grosman, N., Arzy, S., Loewenstein, Y., 2020a. Hierarchical cortical gradients in somatosensory processing. NeuroImage 222, 117257. https://doi.org/10.1016/j.neuroimage.2020.117257
Saadon-Grosman, N., Loewenstein, Y., Arzy, S., 2020b. The ‘creatures’ of the human cortical somatosensory system. Brain Commun. 2. https://doi.org/10.1093/braincomms/fcaa003
Sanchez Panchuelo, R.M., Besle, J., Schluppeck, D., Humberstone, M., Francis, S., 2018. Somatotopy in the Human Somatosensory System. Front. Hum. Neurosci. 12, 235. https://doi.org/10.3389/fnhum.2018.00235
Sanchez-Panchuelo, R.M., Besle, J., Beckett, A., Bowtell, R., Schluppeck, D., Francis, S., 2012. Within-Digit Functional Parcellation of Brodmann Areas of the Human Primary Somatosensory Cortex Using Functional Magnetic Resonance Imaging at 7 Tesla. J. Neurosci. 32, 15815. https://doi.org/10.1523/JNEUROSCI.2501-12.2012
Sanchez-Panchuelo, R.M., Francis, S., Bowtell, R., Schluppeck, D., 2010. Mapping Human Somatosensory Cortex in Individual Subjects With 7T Functional MRI. J. Neurophysiol. 103, 2544–2556. https://doi.org/10.1152/jn.01017.2009
Sanders, Z.-B., Wesselink, D.B., Dempsey-Jones, H., Makin, T.R., 2019. Similar somatotopy for active and passive

digit representation in primary somatosensory cortex. bioRxiv. https://doi.org/10.1101/754648
Schellekens, W., Bakker, C., Ramsey, N.F., Petridou, N., 2020. Moving in on human motor cortex. Characterizing the relationship between body parts with non-rigid population Response Fields. bioRxiv. https://doi.org/10.1101/2020.11.12.379339
Schellekens, W., Petridou, N., Ramsey, N.F., 2018. Detailed somatotopy in primary motor and somatosensory cortex revealed by Gaussian population receptive fields. NeuroImage 179, 337–347. https://doi.org/10.1016/j.neuroimage.2018.06.062
Schellekens, W., Thio, M., Badde, S., Winawer, J., Ramsey, N., Petridou, N., 2021. A touch of hierarchy: population receptive fields reveal fingertip integration in Brodmann areas in human primary somatosensory cortex. Brain Struct. Funct. 226, 2099–2112. https://doi.org/10.1007/s00429-021-02309-5
Schieber, M.H., 2002. Motor cortex and the distributed anatomy of finger movements. Adv. Exp. Med. Biol. 508, 411–416. https://doi.org/10.1007/978-1-4615-0713-0_46
Schieber, M.H., Hibbard, L.S., 1993. How somatotopic is the motor cortex hand area? Science 261, 489–492. https://doi.org/10.1126/science.8332915
Schweisfurth, M.A., Frahm, J., Farina, D., Schweizer, R., 2018. Comparison of fMRI Digit Representations of the Dominant and Non-dominant Hand in the Human Primary Somatosensory Cortex. Front. Hum. Neurosci. 12, 492. https://doi.org/10.3389/fnhum.2018.00492
Siero, J.C.W., Hermes, D., Hoogduin, H., Luijten, P.R., Ramsey, N.F., Petridou, N., 2014. BOLD matches neuronal activity at the mm scale: a combined 7T fMRI and ECoG study in human sensorimotor cortex. NeuroImage 101, 177–184. https://doi.org/10.1016/j.neuroimage.2014.07.002
Smith, S.M., Jenkinson, M., Woolrich, M.W., Beckmann, C.F., Behrens, T.E.J., Johansen-Berg, H., Bannister, P.R., De Luca, M., Drobnjak, I., Flitney, D.E., Niazy, R.K., Saunders, J., Vickers, J., Zhang, Y., De Stefano, N., Brady, J.M., Matthews, P.M., 2004. Advances in functional and structural MR image analysis and implementation as FSL. NeuroImage 23 Suppl 1, S208-219. https://doi.org/10.1016/j.neuroimage.2004.07.051
Stringer, E.A., Qiao, P.-G., Friedman, R.M., Holroyd, L., Newton, A.T., Gore, J.C., Chen, L.M., 2014. Distinct fine-scale fMRI activation patterns of contra- and ipsilateral somatosensory areas 3b and 1 in humans. Hum. Brain Mapp. 35, 4841–4857. https://doi.org/10.1002/hbm.22517
Valente, G., Kaas, A.L., Formisano, E., Goebel, R., 2019. Optimizing fMRI experimental design for MVPA-based BCI control: Combining the strengths of block and event-related designs. NeuroImage 186, 369–381. https://doi.org/10.1016/j.neuroimage.2018.10.080
van der Zwaag, W., Gruetter, R., Martuzzi, R., 2015. Stroking or Buzzing? A Comparison of Somatosensory Touch Stimuli Using 7 Tesla fMRI. PloS One 10, e0134610–e0134610. https://doi.org/10.1371/journal.pone.0134610
Vanni, S., Henriksson, L., James, A.C., 2005. Multifocal fMRI mapping of visual cortical areas. NeuroImage 27, 95–105. https://doi.org/10.1016/j.neuroimage.2005.01.046
Wager, T.D., Nichols, T.E., 2003. Optimization of experimental design in fMRI: a general framework using a genetic algorithm. NeuroImage 18, 293–309. https://doi.org/10.1016/S1053-8119(02)00046-0
Wager, T.D., Vazquez, A., Hernandez, L., Noll, D.C., 2005. Accounting for nonlinear BOLD effects in fMRI: parameter estimates and a model for prediction in rapid event-related studies. NeuroImage 25, 206–218. https://doi.org/10.1016/j.neuroimage.2004.11.008
Wang, L., Zhang, Z., Okada, T., Li, C., Chen, D., Funahashi, S., Wu, J., Yan, T., 2021. Population Receptive Field Characteristics in the between- and Within-Digit Dimensions of the Undominant Hand in the Primary Somatosensory Cortex. Cereb. Cortex 31, 4427–4438. https://doi.org/10.1093/cercor/bhab097
Wang, X., Merzenich, M.M., Sameshima, K., Jenkins, W.M., 1995. Remodelling of hand representation in adult cortex determined by timing of tactile stimulation. Nature 378, 71–75. https://doi.org/10.1038/378071a0
Willoughby, W.R., Thoenes, K., Bolding, M., 2020. Somatotopic Arrangement of the Human Primary Somatosensory Cortex Derived From Functional Magnetic Resonance Imaging. Front. Neurosci. 14, 598482. https://doi.org/10.3389/fnins.2020.598482
Wilson, J.L., Jenkinson, M., de Araujo, I., Kringelbach, M.L., Rolls, E.T., Jezzard, P., 2002. Fast, fully automated global and local magnetic field optimization for fMRI of the human brain. NeuroImage 17, 967–976.